CONTRAST MEDIA & MOLECULAR IMAGING

Received: 10 October 2014, Revised: 24 January 2015, Accepted: 3 February 2015, Published online in Wiley Online Library: 15 April 2015

(wileyonlinelibrary.com) DOI: 10.1002/cmmi.1636

Bioresponsive probes for molecular imaging: concepts and *in vivo* applications

Sander M. J. van Duijnhoven[a,b], Marc S. Robillard[b], Sander Langereis[b] and Holger Grüll[a,b]*

Molecular imaging is a powerful tool to visualize and characterize biological processes at the cellular and molecular level *in vivo*. In most molecular imaging approaches, probes are used to bind to disease-specific biomarkers highlighting disease target sites. In recent years, a new subset of molecular imaging probes, known as bioresponsive molecular probes, has been developed. These probes generally benefit from signal enhancement at the site of interaction with its target. There are mainly two classes of bioresponsive imaging probes. The first class consists of probes that show direct activation of the imaging label (from "off" to "on" state) and have been applied in optical imaging and magnetic resonance imaging (MRI). The other class consists of probes that show specific retention of the imaging label at the site of target interaction and these probes have found application in all different imaging modalities, including photoacoustic imaging and nuclear imaging. In this review, we present a comprehensive overview of bioresponsive imaging probes in order to discuss the various molecular imaging strategies. The focus of the present article is the rationale behind the design of bioresponsive molecular imaging probes and their potential *in vivo* application for the detection of endogenous molecular targets in pathologies such as cancer and cardiovascular disease. Copyright © 2015 John Wiley & Sons, Ltd.

Keywords: bioresponsive agents; activatable probes; molecular imaging; biomarker

1. INTRODUCTION

Molecular imaging involves the noninvasive visualization and quantitative detection of biomolecules *in vivo* by means of target-specific probes (1–5). Valuable applications of molecular imaging are accurate disease detection, phenotyping, and staging by gathering information on molecular pathways underlying biological and cellular processes in the diseased tissue (1–6). Hence, molecular imaging is likely to play a pivotal role in the stratification of patients for personalized treatment. Furthermore, molecular imaging is clinically relevant in the discovery and development of drugs and for the real-time assessment of the efficacy of drug therapy (7,8). Further, it can contribute to improved interventions by image-guided drug delivery and image-guided surgery (9–12). Finally, molecular imaging has an impact in the development of regenerative medicine and stem-cell therapies (6). In most molecular imaging approaches, target-specific molecular probes are engineered to enhance image contrast at the target site. These conventional targeting molecular imaging probes consist of a ligand that binds to an endogenous molecular target and an imaging label for readout. Typically, the molecular imaging probes are designed so that they can be injected intravenously for targeting biomolecules accessible via the blood circulation. For example, the active site of enzymes has been targeted with conventional probes, providing a readout for enzyme abundance (13). However, these probes lack the possibility of detecting enzymatic activity *in vivo* as they are typically limited to a 1:1 probe/target binding fashion. In that respect, a new subset of protease activatable molecular imaging probes has generated considerable attention. These probes have been directed to the active site of the enzymes resulting in the cleavage and activation of the imaging probe (14). Importantly, this will lead to signal amplification since the molecular target can continuously activate the imaging probe and, moreover, it offers a readout of enzyme activity instead of enzyme abundance. Although protease activatable probes have been mainly restricted to fluorescence optical imaging, recent progress has led to the development of protease activatable probes for photoacoustic imaging, magnetic resonance imaging (MRI), and the nuclear imaging modalities single photon emission computed tomography (SPECT) and positron emission tomography (PET) (14–18). Furthermore, activatable molecular imaging probes have also successfully detected other endogenous molecular targets, such as reactive oxygen species (ROS) and metal ions. The purpose of this review is to present a general overview of the rationale behind the design of the multiple types of so-called bioresponsive molecular imaging probes for the detection of a wide range of endogenous molecular target. We will guide the reader through the emerging field of bioresponsive molecular imaging by discussing the various imaging probe strategies and their potential *in vivo* application per imaging modality. For optical imaging and MRI, bioresponsive probes have been reported that show signal amplification by direct activation of the imaging

* *Correspondence to: H. Grüll, Eindhoven University of Technology, Department of Biomedical Engineering, High Tech Campus 11 - Room WBC2p2-65, 5656 AE Eindhoven, The Netherlands. E-mail: h.gruell@tue.nl*

a *S. M. J. van Duijnhoven, H. Grüll*
Department of Biomedical Engineering, Eindhoven University of Technology, Eindhoven, The Netherlands

b *S. M. J. van Duijnhoven, M. S. Robillard, S. Langereis, H. Grüll*
Department of Minimally Invasive Healthcare, Philips Research, Eindhoven, The Netherlands

Biographies

Sander van Duijnhoven earned his PhD in biomedical engineering from the Eindhoven University of Technology, The Netherlands, in 2012, where his research focused on activatable cell-penetrating imaging probes. Sander is currently pursuing a postdoctoral research training at the Radboud University Medical Center Nijmegen, The Netherlands. Furthermore, he is currently employed by Tagworks Pharmaceuticals, The Netherlands. His current research efforts focus on the development and application of targeted therapy agents and molecular imaging probes that improve therapy and/or diagnosis of disease.

Marc Robillard obtained his PhD in bio(in)organic chemistry at the Leiden Institute of Chemistry, The Netherlands, in 2003. Marc is founder and CEO of Tagworks Pharmaceuticals, a spin-out of Philips Research Europe. Tagworks develops and applies bioorthogonal conjugation and elimination chemistry in living systems to improve the efficacy of cancer therapies and to enable novel approaches in companion diagnostics. Prior to spinning out in 2011 he worked at Philips Research on molecular imaging and drug delivery and at Kreatech Diagnostics on microarray detection.

Sander Langereis received his PhD in chemistry at the Eindhoven University of Technology in 2005, where his research focused on target-specific dendritic magnetic resonance imaging (MRI) contrast agents. His research activities span the range of responsive MRI contrast agents, paramagnetic self-assembled nanosystems, and novel drug delivery systems. Sander moved to Philips Research Europe, where his research focuses on new approaches for localized drug delivery under MR image guidance. Ultrasound-mediated drug delivery using high intensity focused ultrasound and temperate-sensitive liposomes are of particular interest.

Holger Grüll received his PhD in chemistry from University of Cologne, Germany, in 1996. Subsequently he spent two years at the National Institute of Standards and Technology, MD, USA, and one year at the Ben Gurion University of the Negev, Israel, before joining Philips Research, the Netherlands, in 2000. In 2007, Holger was appointed part time professor at the Eindhoven University of Technology with a chair in molecular imaging and image-guided therapy. His research interests are on new probes for molecular imaging, responsive probes for drug delivery and high intensity focused ultrasound.

label (i.e. probes that go from an "off" to an "on" state) or by specific retention of the imaging probe at the site of interaction through a specific biological or chemical mechanism. Bioresponsive probes for photoacoustic imaging and SPECT/PET have been typically designed to show local retention and accumulation at the site of interaction.

2. BIORESPONSIVE OPTICAL PROBES: ACTIVATION OF THE OPTICAL IMAGING LABEL

2.1. Protease sensitive bioresponsive optical probes

Proteases play crucial roles in physiology and pathology and have been identified as attractive targets for molecular imaging of a variety of diseases, including cancer, atherosclerosis, myocardial infarction, and neurological diseases (14–19). Multiple types of protease bioresponsive optical probes have been developed in the past decades that are specifically directed at the activity of the enzyme instead of enzyme abundance. These probes include fluorescent autoquenched probes, self-quenched or homo-fluorescence resonance energy transfer (homo-FRET) probes, dual-labeled FRET probes, fluorescent quenched activity-based probes, and luminescent probes (14–19).

2.1.1. *Fluorescent autoquenched probes*

An autoquenched probe typically consists of a peptide substrate linked via an amide to fluorescein/rhodamin spirolactam or spirolactone derivative, which is essentially optically silent (20). The probe regains its fluorescence upon conversion of the amide moiety into an amine and subsequent ring-opening of the corresponding spirolactam/lactone (11,21–24) (Fig. 1). For example, a caspase-3 and −7 autoquenched probe was designed by conjugating the peptide substrate DEVD to a rhodamine spirolactone derivative. Release of DEVD peptide by intracellular caspase-3 or −7 resulted in ring-opening of the spirolactone, followed by a strong enhancement of fluorescence (25) (Scheme 1). A γ-glutamyltranspeptidase autoquenched probe was successfully used for the endoscopic detection of γ-glutamyltranspeptidase *in vivo* in a mouse model of colon cancer (11,26). Recently, a novel self-immolative autoquenched probe has been described. Here, a naphthalimide dye was conjugated via an electron-withdrawing self-immolative linker to a trigger group yielding

Figure 1. Autoquenched probe. Attachment of a protease substrate to a fluorophore is designed to result in a nonfluorescent structure. Proteolytic removal of the substrate results in the restoration of fluorescence.

an autoquenched probe. Elimination of the self-immolative linker by enzymatic removal of the trigger yielded a highly fluorescent dye (27).

So far, these autoquenched probes use fluorophores that emit light in the visible region. Compared to visible light, near-infrared (NIR) radiation penetrates tissues more efficiently, up to several centimeters, and shows decreased absorption by natural proteins like hemoglobin (15,28,29). Therefore, the development of autoquenched probes based on NIR fluorophores would be an interesting strategy to broaden the applications of these autoquenched probes *in vivo*.

2.1.2. *Fluorescent self-quenched probes*

Self-quenched probes or homo-FRET probes are typically macromolecular imaging probes that make use of multiple NIR fluorophores that are in close proximity to each other. When excited, the fluorophores absorb energy from each other resulting in self-quenching. The efficiency of energy transfer between the fluorophores is given by:

$$E = \frac{R_0^6}{R_0^6 + r^6} \quad (1)$$

where r is the distance between the fluorophores and R_0 is the Förster distance (30). The Förster distance is the distance at which the energy transfer efficiency is 50% and is typically in the range of 2–6 nm. Proteolytic activation of these probes liberates the fluorophores, resulting in the loss of homo-FRET, activating fluorescence.

Weissleder and coworkers functionalized a poly-L-lysine backbone with methoxy-terminated poly(ethylene glycol) and multiple self-quenched NIR Cy5.5 fluorophores. Degradation of the poly-L-lysine backbone by lysosomal cysteine/serine proteases resulted in liberation and activation of the fluorophores (31–35). The range of applications of these macromolecular probes (~450 kDa), was extended by inclusion of various peptide substrates between the fluorophores and the backbone (Fig. 2). Following this approach, activatable probes were developed for a variety of enzyme targets like caspase-1, cathepsins D, E and K, HIV-1 protease, urokinase, and matrix metalloproteinases (MMPs) subtype 2 and 9 (36–47). For example, MMP-2 selectivity was achieved by inserting the MMP-2 sensitive peptide sequence GPLG-VRGK between the backbone and the fluorophore (44). This probe showed a threefold enhancement in NIR fluorescence signal in tumor xenografts overexpressing MMP-2, compared to tumor xenografts that were treated with an MMP inhibitor (Fig. 2). These self-quenched macromolecular imaging probes have been applied for *in vivo* protease detection in cancer, atherosclerosis, arthritis, and heart failure in rodent models (31–52). Two of these macromolecular probes, one sensitive towards MMPs (MMPSense^{TM}) and the other towards cathepsins (ProSense^{TM}), are commercially available. Recently, a series of self-quenched probes that comprise a novel architecture termed FAST^{TM} (fluorescent activatable sensor technology) have become commercially available. In these probes, an enzyme-sensitive peptide sequence containing NIR fluorochromes at both the C and N terminus is linked to a polymer carrier at a ratio of one substrate per polymer molecule (53). The NIR fluorophores show ~95% self-quenching while the substrate is intact, but become highly fluorescent upon enzymatic cleavage of the substrate. These FAST^{TM} self-quenched probes (~43 kDa) are significantly smaller in size compared to the macromolecular poly-L-lysine-based probes and therefore display an improved pharmacokinetic profile that enables *in vivo* molecular imaging at earlier time-points. These probes have successfully been used for the detection *in vivo* of the proteolytic activity of renin, MMPs, cathepsin B, and neutrophil elastase (52–59).

In recent years, several other activatable self-quenched fluorescent imaging probes have been developed for protease sensing. An MMP-9 sensitive liposomal system was developed that showed *in vitro* protease-triggered release and activation

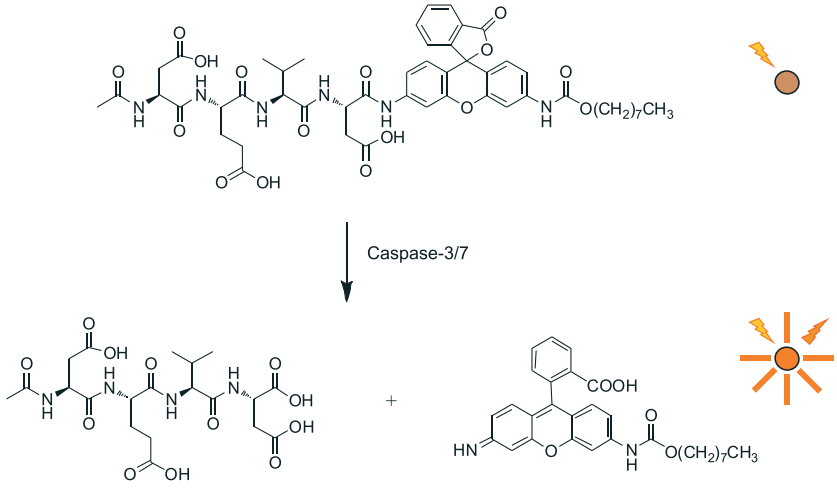

Scheme 1. A caspase-3/7 sensitive autoquenched probe. The rhodamine fluorophore is activated upon release of the DEVD peptide substrate by caspase-3/7 (25).

A

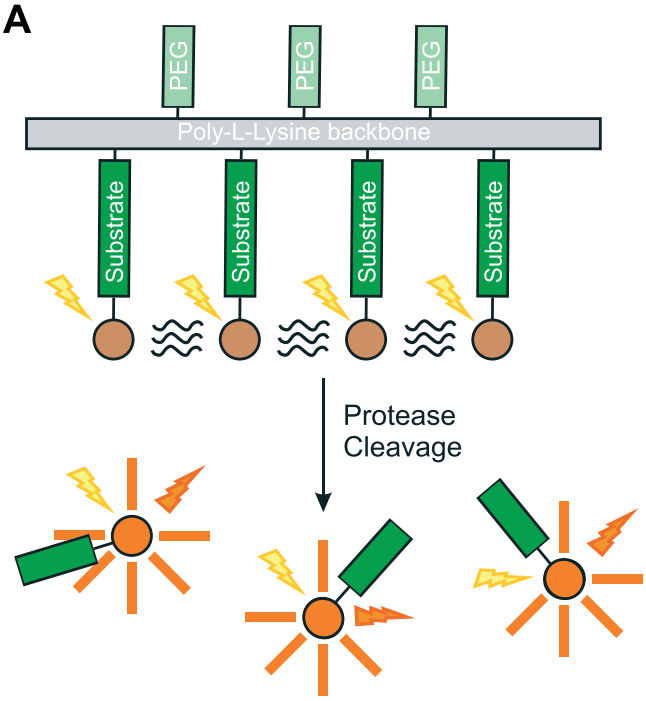

B

Protease	Substrate	Ref
Caspase-1	GWEHD-GK	36
Cathepsin D	GPIC$_{Et}$F-FRLGK	37
Cathepsin E	AGFSL-PAGC	38
Cathepsin K	GHPG-GPQK	39
HIV-1 protease	GVSQNY-PIVGK	40
Urokinase	GGSGR-SANAK	41
MMP-2	GPLG-VRGK	42-45
MMP-2 / MMP-9	GGPRQ-ITAG	46,47

C

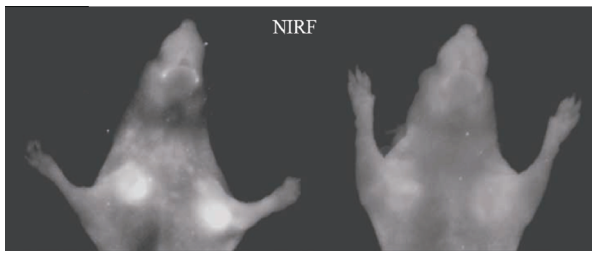

Figure 2. (A) Schematic representation of a self-quenched polymer-based probe. Multiple fluorophores coupled to a backbone lead to self-quenching of the fluorophores. Upon proteolytic degradation of the probe, the fluorescence is restored. (B) The table shows applied peptide substrates resulting in the development of a variety of enzyme-specific self-quenched probes (36–47). (C) *In vivo* NIR fluorescence image of MMP-2 positive HT-1080 tumor-bearing animals using a MMP-2 sensitive self-quenched probe. A threefold higher fluorescent signal was observed in tumors of untreated tumor-bearing mice (left) compared to tumor-bearing mice that were treated with the MMP inhibitor prinomastat (right). Figure C is reprinted with permission from (44).

of encapsulated fluorophores in the presence of MMP-9 (60,61). Here, MMP-9 cleavable lipopeptides were incorporated into the liposome bilayer. Degradation of the lipopeptide resulted in destabilization of the bilayer and subsequent leakage and activation of the fluorescent dyes that were present in the lumen of the liposomes (Fig. 3).

Another approach of activatable self-quenched probes focussed on the protease triggered release and activation of fluorophores from a nanofiber precursor for the detection of urokinase activity (62). The probe comprised a self-assembling peptide sequence to which a fluorophore was coupled via a urokinase-sensitive peptide moiety. Spontaneous self-assembly of the peptide probe resulted in an optically quenched nanofiber, in which the fluorophore was released and activated upon urokinase digestion *in vitro*. In a similar approach, a NIR triple helical peptide-based optical probe was developed. Each peptide strand was flanked by two NIR fluorescent dyes. In the triple-helical structure, the fluorescence was reduced due to quenching. *In vivo* studies in tumor-bearing mice showed MMP-mediated degradation of the triple-helical peptide in tumors, resulting in the local release of fluorophore labeled peptides and amplification of the fluorescent signal (63).

Finally, self-quenched fluorophore-encapsulated nanogels have been developed that showed release and activation of the fluorophore upon nanogel degradation by hyaluronidase (64).

2.1.3. *Fluorescent dual-labeled FRET probes*

The common feature of protease-sensitive dual-labeled FRET-based molecular imaging probes is the loss of FRET between a donor fluorophore and a distinct acceptor fluorophore or nonfluorescent quencher upon enzymatic degradation of a substrate initially holding the fluorophores together. For the former class, the distance between the two distinct fluorophores, typically smaller than Förster radius (eqn 1), results in efficient FRET from the donor fluorophore to an acceptor fluorophore predominantly yielding light emission of the acceptor fluorophore. Proteolysis of the peptide substrate results in separation of the fluorophores and loss of energy transfer (Fig. 4A). These dual-wavelength probes can be used for ratiometric imaging, which provides accurate quantification of probe activation. For the second class, efficient energy transfer will take place between the donor fluorophore and a nonfluorescenct quencher, resulting in a low fluorescent signal from the donor fluorophore. Degradation of the substrate results in the dissociation of the fluorophore–quencher pair and leads to a significant enhancement in fluorescence (Fig. 4B). A wide variety of single-wavelength and ratiometric FRET probes has been described in literature (59,65–95).

Genetically encoded fluorescent sensors consisting of two distinct fluorescent proteins are generally aimed at the colorimetric detection of intracellular proteases such as caspases or kinases (65,66). These probes typically consist of a protease cleavable substrate (65) or a conformationally responsive domain (66) sandwiched between two mutants of the green fluorescent protein (GFP) capable of FRET. Degradation of the cleavable substrate or a protease-induced conformational change of the linker domain is associated with a change in distance between the two fluorescent proteins and thus a change in FRET. For example, a genetically encoded caspase-sensitive FRET probe consisted of a cyan fluorescent protein (CFP) and a yellow fluorescent protein (YFP) joined by a peptide domain sensitive for caspase-1 or

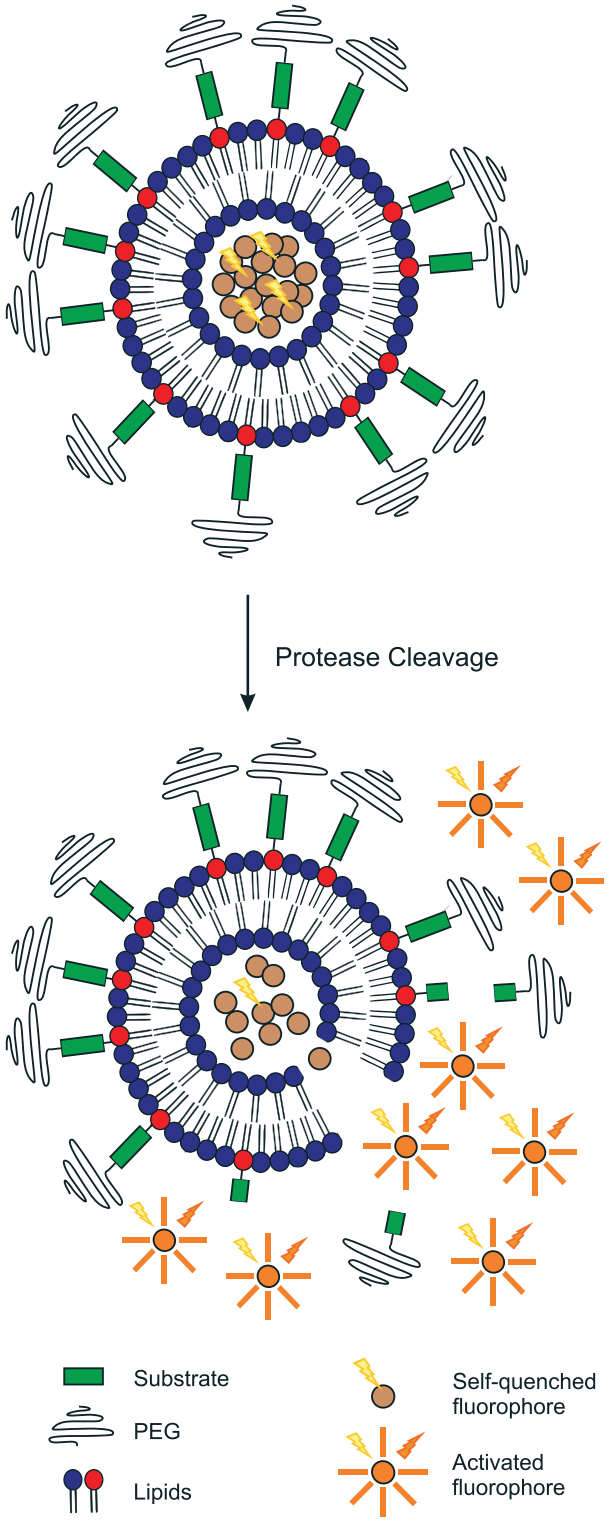

Figure 3. Depiction of a self-quenched probe based on protease-degradable liposomes. Multiple fluorophores encapsulated in the aqueous lumen of a liposome lead to self-quenching of the fluorophores. Upon proteolytic degradation, the liposomes fall apart and the fluorophore is released, resulting in restoration of fluorescence.

caspase-3 (65). Proteolysis of the peptide domains significantly enhanced the distance between CFP and YFP, and resulted in a decrease in FRET. Recently, novel genetically encoded biosensors have been reported that visualize MMPs at the extracellular

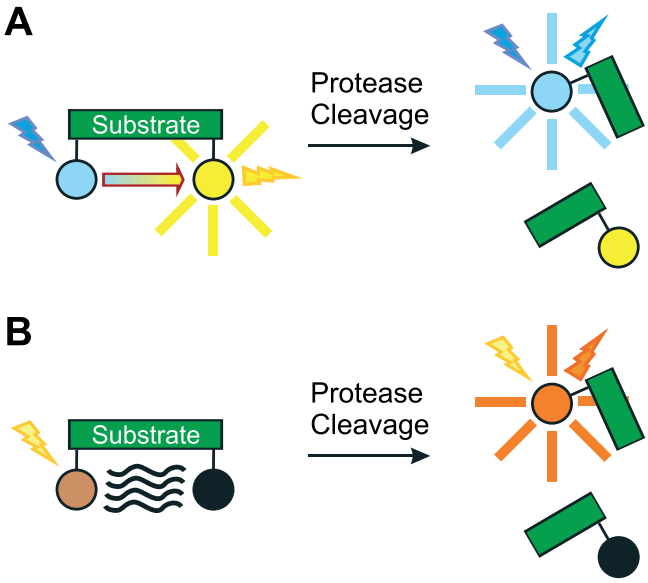

Figure 4. Dual-labeled FRET-based probes, based on protease substrates labeled with (A) two distinct fluorophores or (B) a fluorophore-quencher pair.

surface of the cell membrane (67–69). Although recent progress led to the development of NIR fluorescent proteins enabling deep tissue imaging (96,97), the need for gene transfection is a strong limitation to clinical application in humans. However, it is a powerful research tool in the preclinical setting.

In other strategies, organic NIR fluorophores have been successfully employed in low molecular weight activatable FRET-based probes. For example, an MMP-7 peptide substrate was flanked with the organic Cy5.5 fluorophore and the organic NIR quencher NIRQ820 (70). A sevenfold increase in fluorescence was observed upon incubation with MMP-7. Recent research has resulted in the development of activatable organic FRET probes specifically targeting extracellular proteases (59,71–83). One of these probes, a membrane-type MMP sensitive probe, consisting of the MMP-14 peptide substrate GRIGF-LRTAKGG and a Cy5.5/BHQ-3 NIR dye-quencher pair, was successfully used to detect MMP-14 activity in tumor-bearing mice (Fig. 5) (79). Moreover, intracellular enzymes have been effectively targeted with organic activatable FRET imaging probes (84–89). For example, cell-permeable caspase activatable probes were developed for the noninvasive detection of apoptosis *in vivo* (84–88). These probes consisted of a Tat-peptide-based permeation sequence and a caspase recognition sequence (DEVD) flanked by a NIR dye-quencher pair.

A special subclass of FRET probes are the fluorescent quenched activity-based probes (ABPs) (90). Fluorescent quenched ABPs undergo an enzyme-catalyzed chemical reaction resulting in a covalent bond between the catalytic site and the probe. This reaction is furthermore characterized by a nucleophilic displacement of the quencher group, resulting in activation of the fluorescent tag. In contrast to the classic FRET probes, the molecular target cannot continuously activate ABP probes due to the covalent bond formation. Nevertheless, cysteine cathepsin activity has successfully been detected *in vivo* with fluorescent quenched ABPs (91,92).

Apart from organic fluorophores, inorganic particles like quantum dots and gold nanoparticles have recently been exploited as

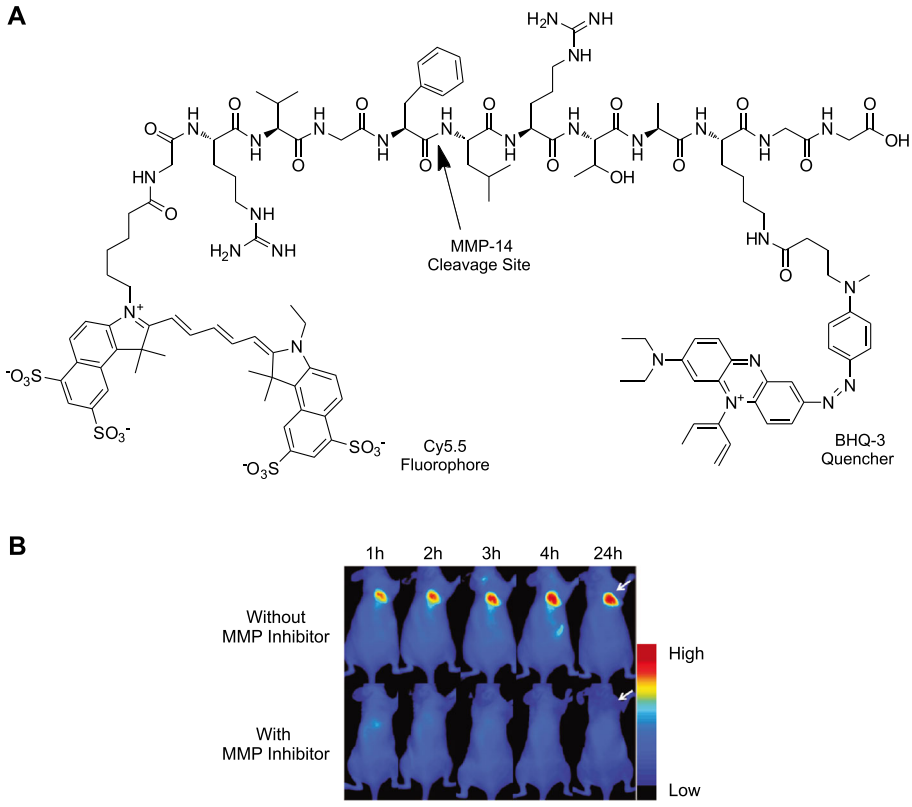

Figure 5. (A) Molecular structure of the MMP-14 substrate GRIGF-LRTAKGG flanked by the NIR dye Cy5.5 and the NIR quencher BHQ-3. (B) *In vivo* NIR fluorescence image of MMP-14-positive MDA-MB-435 tumor-bearing animals using the MMP-14 FRET probe. A three- to fourfold higher fluorescent signal was observed in tumors of untreated mice (top row) compared to mice that were treated with the MMP inhibitor prinomastat (bottom row). Figure B is reprinted with permission from Zhu *et al.* (79). Copyright 2011 American Chemical Society.

donor and acceptor pairs for energy-transfer-based imaging probes (93,94). Gold nanoparticles demonstrated a 71% reduction of quantum dot photoluminescence, as was shown for an MMP activatable quantum-dot-based luminescent probe (95). Quantum dots have advantages over organic fluorophores, such as strong fluorescence, higher photostability against bleaching and changes in physical environment, such as temperature and pH, and a narrow emission bandwidth (98). Nevertheless quantum dots may have limitations for *in vivo* use due to potential cellular toxicity associated with Cd^{2+} or Se^{2-} ion release from the quantum dot core (99). Recent studies, however, indicated that potential toxicity is of minor importance for relatively small nanoparticles, such as quantum dots and chemical dots, which are efficiently cleared by the kidney's thus avoiding extensive liver and spleen uptake (100,101). Specifically, quantum dots with a hydrodynamic diameter smaller than 5.5 nm showed efficient renal excretion (101).

Recently, the principles of FRET imaging and photodynamic therapy (PDT) have been combined into the development of enzyme activatable photodynamic molecular beacons (102–106). In photodynamic therapy (PDT), the cytotoxic agent $^1O_2$ is generated by light activation of a photosensitizer in the presence of oxygen (107). Furthermore, NIR light emission from the photosensitizer is typically observed. Activatable photodynamic molecular beacons have been developed for MMP-7, caspase 3, and fibroblast activation protein, by flanking enzyme-specific substrates with a photosensitizer and a fluorescence/$^1O_2$ quencher (103–106). NIR fluorescence imaging of a MMP-7 sensitive photodynamic molecular beacon showed tumor-specific activation *in vivo*, suggesting tumor-specific delivery of the photosensitizer, which potentially will contribute to improved tumor-specific photodynamic therapy (103).

2.1.4. *Bioresponsive luminescent probes*

Bioluminescence is typically observed upon enzymatic oxidation of specific substrates by luciferases (108). In bioluminescence imaging, the light production does not rely on external excitation, and therefore background signals due to tissue autofluorescence are not present. Luminescent activatable probes, known as caged luciferase substrates, combine the production of bioluminescence by luciferases with the enzymatic activity of other proteases. In these probes, D-luciferin, the substrate for luciferase, is typically protected by a specific enzymatic trigger (Scheme 2). The presence of the enzymatic trigger prevents the enzymatic oxidation of the probe by luciferase. However, upon enzymatic digestion of the trigger, D-luciferin is released and will produce a bioluminescent signal once consumed by luciferase. *In vivo*, luminescent activatable probes have successfully been employed to visualize a variety of enzymes, including β-galactosidase (reporter enzyme), β-lactamase, caspase, and furin (109–112). A recent study demonstrated that D-cysteine and 2-cyanobenzothiazoles (CBT) selectively react with each other *in vivo* to yield D-luciferin (113). A bioresponsive luminescent probe was developed by conjugating D-cysteine to a caspase 3/7 substrate. *In vivo* release of D-luciferin from the caspase 3/7 sensitive probe in luciferase-expressing tumor-bearing mice allowed the reaction with administered 6-amino-CBT to form

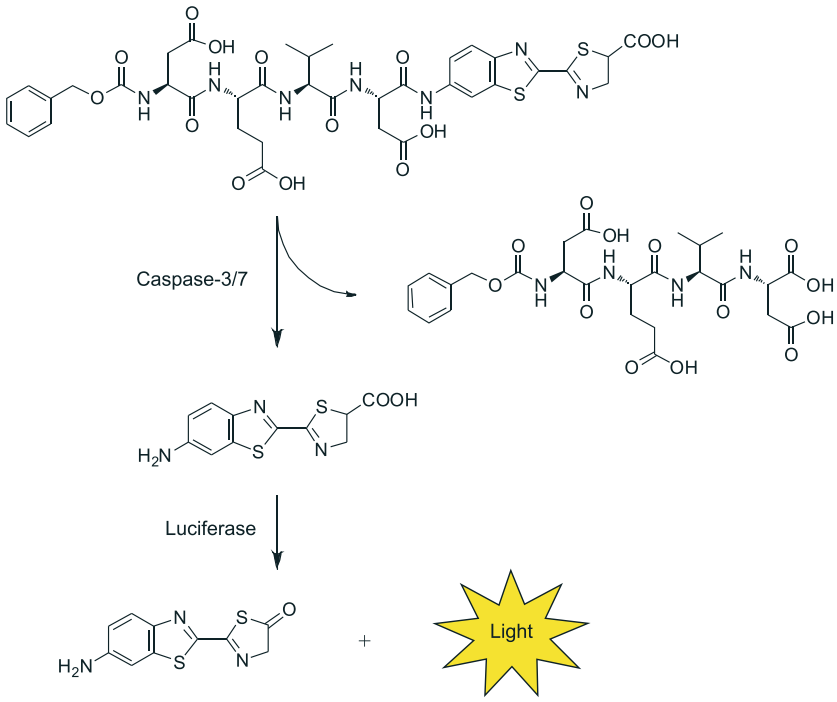

Scheme 2. A caspase-3/7 sensitive activatable bioluminescent probe. D-luciferin is released upon cleavage of the DEVD peptide substrate by caspase-3/7 and is subsequently consumed by luciferase, resulting in a bioluminescent signal (111).

6-amino-D-luciferin. Subsequently reaction of 6-amino-D-luciferin with luciferase yielded a bioluminescent signal (113). Similar to fluorescent genetically encoded FRET probes, activatable luminescent probes are valuable for preclinical studies, but clinical translation is restricted due to the need for gene transfection of the luciferase gene. Interestingly, a recent study has demonstrated that it may become possible to enlist endogenous enzymes from nonluminescent organisms such as luciferases, circumventing the need for genetic manipulation (114).

2.2. pH-sensitive optical probes

The important role of intracellular pH in cell, enzyme, and tissue activity as well as the recognition that the tumor's extracellular microenvironment is relatively acidic compared to normal tissue has stimulated the development of pH-sensitive fluorescent imaging probes (115–129). On average, the pH in the tumor microenvironment is between 6 and 7 (130). In the early days, pH-dependent probes were aimed at the enhancement of fluorescence of the GFP upon a decrease in pH (110). Other strategies focussing on pH-dependent activation of the fluorescent imaging label used pH-sensitive nanoparticles, for example, liposomes or polypeptides that showed release and activation of fluorescence of self-quenched fluorophores at low pH (119–121). More recently, low molecular weight pH-sensitive autoquenched fluorescent probes have been developed (Fig. 6). Most of these probes are specifically targeted to tumors and become fluorescent once accumulated in acidic lysosomes, typically having a pH varying from 4 to 6 (122–128). For example, a near-infrared pH-activatable fluorophore conjugated to a RGD-peptide was successfully used for the targeting of $\alpha_v\beta_3$ integrin-expressing tumors (124). Subsequent $\alpha_v\beta_3$ integrin-mediated internalization of the probe into acidic lysosomes resulted in an enhancement of fluorescence. Recently, a self-assembled self-quenched imaging probe has been developed that showed efficient disassembly and activation of fluorescence at pH $<$ 7.0 (129).

2.3. Optical probes activated by reactive oxygen/nitrogen species

Reactive oxygen species and reactive nitrogen species (RNS) play a crucial role in maintaining normal physiology. However, excessive production of ROS/RNS has been associated with a variety of pathological diseases, such as cancer and cardiovascular disease (131,132). Activatable fluorescent imaging probes for ROS/RNS detection are mainly based on autoquenched probes in which a fluorophore is coupled to a ROS/RNS trigger, resulting in a nonfluorescent molecule (20,133). Reaction of these probes with ROS/RNS results in the activation of the fluorescent moiety (Scheme 3). This approach has been extensively exploited, resulting in activatable fluorescent probes for a range of ROS/RNS, including hydrogen peroxide (H_2O_2) (134–141), peroxynitrite ($ONOO^-$) (142–146), superoxide (O_2^-) (147–149), nitric oxide (NO) (150–152), hypochlorous acid (HOCl) (142–144,153–155), and hydroxyl radical (·OH) (144,156). Other imaging approaches have focussed on the colorimetric detection of ROS/RNS (157–160) or used genetically encoded biosensors (161–163).

ROS/RNS imaging methods have been applied in cell-culture experiments *in vitro*, but strategies to visualize ROS/RNS *in vivo* have been limited (142,164–167). The first *in vivo* study employed nanoparticles formulated from peroxalate esters and fluorescent dyes (164). Reaction of the peroxalate esters with H_2O_2 resulted in high-energy dioxetanedione intermediates that subsequently facilitated excitation of the encapsulated dye. This probe was used to detect H_2O_2 in the peritoneal cavity of mice during a lipopolysaccharide-induced inflammatory response. H_2O_2 production was also visualized in tumor-bearing mice using a peroxy-caged luciferin-1 bioluminescent probe (165). Selective reaction of this probe with H_2O_2 released firefly

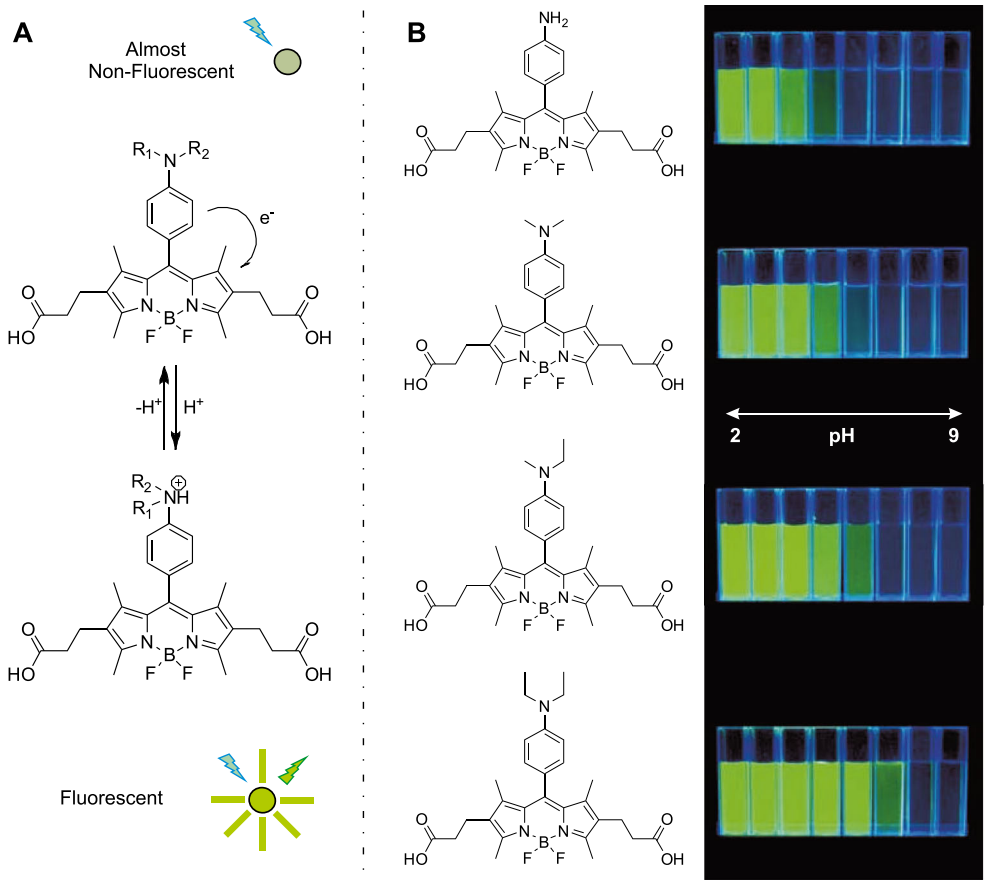

Figure 6. (A) Reaction mechanism showing the reversible pH-dependent fluorescence activation of a pH-sensitive optical probe. In the native state, the probe is essentially nonfluorescent due to intramolecular photon-induced electron transfer from the aniline moiety to the fluorophore. Once protonated, the probe becomes highly fluorescent. (B) pH profiles of fluorescence for various pH-sensitive fluorescence probes. The pH ranges from 2 (left) to 9 (right) in single pH unit increments. Figure B is reprinted (adapted) with permission from (122).

luciferin that subsequently was converted to a bioluminescent active moiety by firefly luciferase. This probe was studied in luciferase-expressing tumor-bearing mice and showed tumor-specific activation. In a follow-up study, a dual-analyte bioluminescent strategy was developed for the simultaneous detection of H_2O_2 and caspase (166). In this approach, two complementary bioorthogonal caged precursors (6-hydroxy-2-cyanobenzothiazole (HCBT) and D-cysteine) were unmasked by, respectively, H_2O_2 and caspase 8. After their release, the HCBT and D-cysteine cages react with one another and form luciferin, producing a bioluminescent signal upon reaction with luciferase. An *in vivo* study in a luciferase-expressing mouse model of inflammation demonstrated proof-of-concept for this dual-analyte detection technology (166). Panizzi *et al*. developed a ROS/RNS nanoparticle to which quenched oxazine reporters were conjugated (142). Release of the oxazine reporters by ROS/RNS interaction, in particular $ONOO^-$ and HOCl, resulted in restoration of its fluorescence. This nanoparticle was studied in a mouse model of myocardial infarction and showed enhancement of oxazine fluorescence in the infarcted areas of the heart. Lastly, a H_2O_2 ratiometric FRET probe has recently been developed employing fluorescein and Cy-5 as a donor/acceptor FRET pair (167). Reaction of this probe with H_2O_2 led to a decrease in FRET and subsequent increase in fluorescein fluorescence, as was demonstrated *in vitro* and *in vivo* in a mouse model of lung inflammation.

2.4. Optical probes activated upon target binding

The final class of bioresponsive fluorescent imaging probes shows a change in FRET between a donor fluorophore and acceptor fluorophore or quencher upon target binding. For instance, various genetically encoded FRET sensors based on GFP-mutants undergo a conformational change upon target binding and allowed the *in vitro* ratiometric detection of, for example ATP, glucose, and metal ions like calcium, zinc, and cadmium (168–172). Another strategy is focussed on FRET oligonucleic acid-based aptamer probes in which a fluorescent label is efficiently activated upon a conformational change of the probe induced by binding to a biomarker (Fig. 7) (173,174). Alternatively, micellar and liposomal formulations containing high concentrations of self-quenched fluorescent dyes have been developed that destabilize and release the fluorescent dyes upon target binding, cellular internalization, and subsequent nanocarrier degradation (175,176). Similarly, various FRET probes have been developed that upon target binding and subsequent cellular internalization showed activation of the optical imaging label (177–179).

2.5. Fluorescence lifetime imaging

For most fluorescence techniques, the increased fluorescence intensity upon activation of the optical imaging probe is used as a

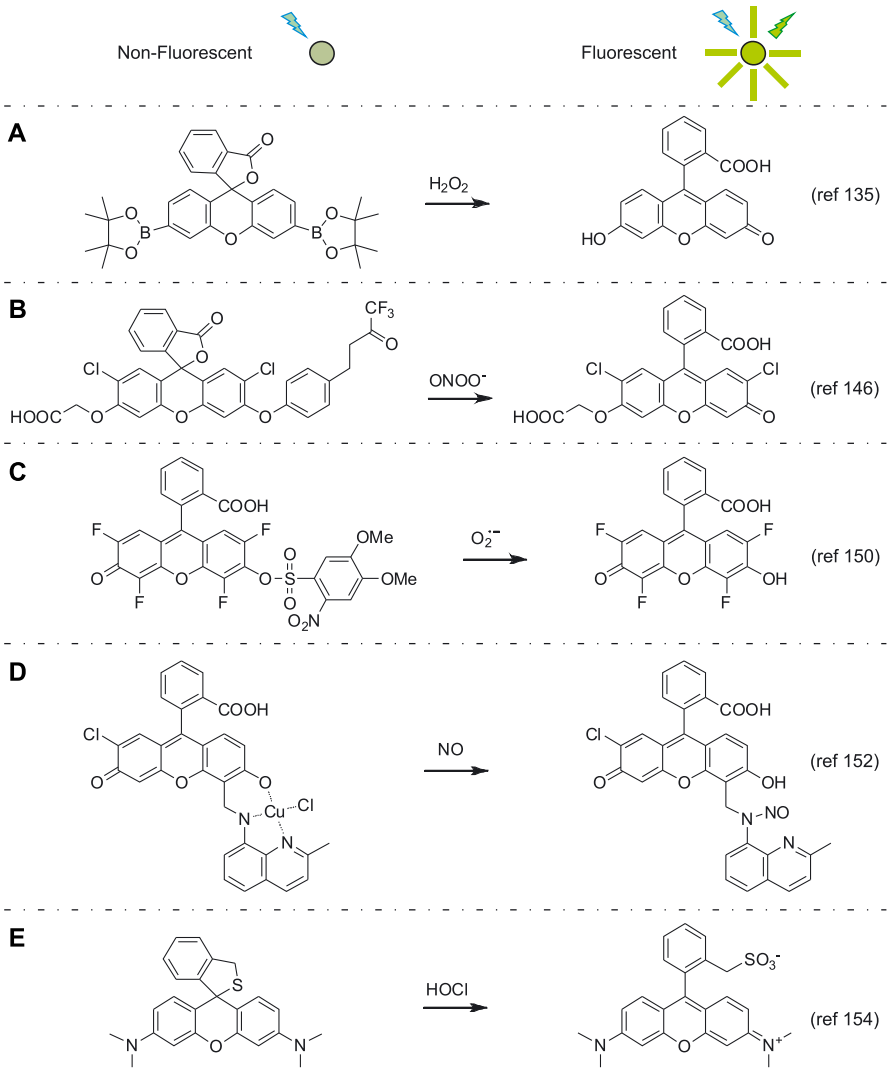

Scheme 3. Reaction mechanism of various ROS/RNS activatable fluorophores. Shown are turn-on fluorescein derivatives for (A) H_2O_2, (B) $ONOO^-$, (C) $O_2^{\cdot-}$, (D) NO, and (E) HOCl.

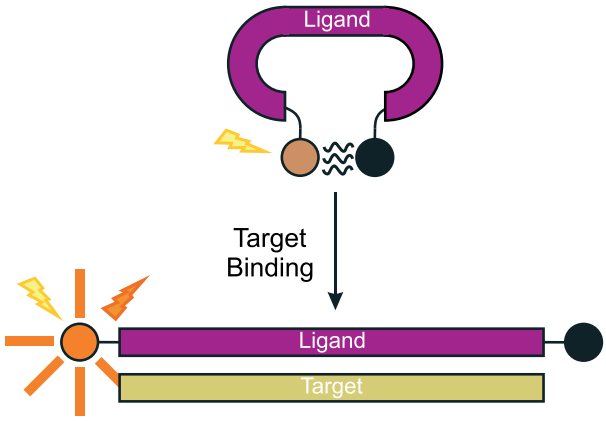

Figure 7. Schematic representation of an activatable aptamer probe. In the absence of a target, the probe is typically in a hairpin conformation, resulting in quenched fluorescence. Upon target binding, its conformation is altered, resulting in activation of the fluorophore.

measure of activation. Next to fluorescence intensity, the fluorescence lifetime (FLT) properties of the fluorophores change due to activation of the probe (180). The fluorescence lifetime describes the length of time between the excitation of a fluorophore and subsequent fluorescent emission and can be influenced by changes in the environment. For example, energy transfer between the donor and acceptor fluorophore in FRET-based imaging probes results in a lower quantum yield as well as decrease of the fluorescence lifetime of the donor fluorophore (181). Upon probe activation, the quantum yield and lifetime are restored, resulting in an increase in fluorescence intensity and lifetime of the donor fluorophore. Consequently, monitoring the fluorescence lifetime can be utilized to assess whether *in vivo* probe activation has occurred (182).

2.6. Clinical application of optical imaging probes

The previous paragraphs present an overview of bioresponsive optical imaging probes. A unique feature of optical imaging is that the imaging probes can be turned on upon activation by a specific endogenous molecular target, allowing high target-to-background ratios compared to conventional targeting probes.

Unfortunately, the limited depth of light penetration through human tissue hampers the application of optical imaging probes for image-based whole-body diagnostics *in vivo*. However, in recent years these probes have been demonstrated to have a high potential in intraoperative imaging approaches of surface-located tissues, such as those encountered during endoscopic or optically guided surgical interventions (6,10–12,183–185). A first study in a human showed the efficacy of a folate receptor-α targeting non-NIR fluorescence imaging probe for image-guided tumor margin detection during cancer surgery (186). This study and various other studies provide essential proof-of-principle that intraoperative optical imaging holds great promise to become a standard clinical tool in cancer treatment (186–197). While the pioneering studies in a human employed targeted optical imaging probes, multiple bioresponsive optical imaging probes are currently also in the process of obtaining regulatory approval for clinical proof-of-principle studies (198).

3. BIORESPONSIVE PHOTOACOUSTIC IMAGING PROBES

It has been shown recently that NIR fluorophores can also be used for photoacoustic tomography (PAT) (199). This technique, which is one of fastest growing imaging modalities in recent years (200), is based on the monitoring of ultrasonic signals generated in response to light absorption properties of specific endogenous molecules, such as hemoglobin or exogenously administered imaging probes. In more detail, photoabsorbing molecules absorb light from nonionizing laser pulses, resulting in subsequent energy dissipation as heat. This process subsequently leads to thermal expansion and emission of broadband acoustic waves. The ultrasonic waves can be detected with adequate ultrasonic transducers, up to several centimeters in large animals and humans (15). The signal is subsequently processed with reconstruction algorithms to recover the initial absorbed energy distribution. Thus, photoacoustic imaging is a hybrid technique making use of optical absorption and ultrasonic wave propagation. Thereby, photoacoustic imaging combines the advantages of both techniques: the high contrast of optical imaging and the high resolution of ultrasonic imaging, which offers great promise for this novel imaging modality in future clinical applications (15). An optimal photoacoustic imaging probe is characterized by a high extinction coefficient that furthermore possesses efficient conversion of the electromagnetic energy into mechanical energy. Despite NIR fluorescent dyes that do show fluorescence, these chromophores have been proven to be attractive for photoacoustic imaging because of their relatively low quantum yield. Therefore, a major part of the absorbed energy, more than 80%, is transferred to optoacoustic signals (201). Furthermore, the specific use of NIR chromophores as photoacoustic imaging agents in combination with excitation light of a corresponding wavelength allows background signal suppression, because of the low absorbance of endogenous photoabsorbers present in normal tissue in the NIR wavelength window (15). In recent years, several bioresponsive photoacoustic imaging probes have been developed. Razansky *et al*. explored the use of MMPSense™ 680 for multispectral photoacoustic imaging (201). They demonstrated that the chromophores in MMPSense™ 680 show an absorption change upon enzymatic activation, which could be detected by multispectral photoacoustic imaging at 635 and 675 nm. This approach allowed high accurate three-dimensional photoacoustic imaging of MMP activity in human carotid plaques (201). In other work, Levi *et al*. developed an MMP activatable cell-penetrating peptide labeled with two chromophores, BHQ3 and Alexa750, which show photoacoustic signals upon laser irradiation at 675 and 750 nm respectively (202). It was demonstrated that activation of the imaging probe *in vitro* resulted in efficient cellular uptake of the cell-penetrating peptide domain labeled with BHQ3, while the counterpart containing Alexa750 diffused away, as was confirmed by photoacoustic signal intensity of both chromophores (202). This probe was subsequently explored *in vivo* and multispectral photoacoustic imaging was used to detect tumor-associated MMP activity in mice (203). In another study, ratiometric multispectral photoacoustic imaging using an activatable imaging nanoprobe was successfully demonstrated for detection of cancer-associated MMP activity *in vivo* (204). The nanoprobe consisted of multiple chromophores BHQ-3 that were conjugated via MMP cleavable linkers to copper sulfide nanoparticles. Both BHQ-3 and the copper sulfide nanoparticles, which exhibit distinctive absorption peaks at 680 nm and 930 nm respectively, generate optoacoustic signals upon laser radiation. Activation of this nanoprobe by tumor-associated MMPs resulted in the release and tumor wash-out of the small molecular weight BHQ-3 molecules, while the large CuS nanoparticles were retained for much longer in the tumor. Multispectral photoacoustic imaging of the signal ratio 680 nm/930 nm consequently showed a decrease in ratio in tumor tissue *in vivo* and demonstrated the use of this probe for proteinase activity detection *in vivo* (204). Lastly, novel activatable photoacoustic probes have been developed for photoacoustic lifetime imaging (205–207). In one strategy, a protease sensitive imaging probe has been proposed that contains self-assembled methylene blue chromophores. Upon enzymatic activation, the chromophore monomers will be released, which will result in a change in the excited state lifetime of the chromophore (205). The same chromophores demonstrated pO_2 dependent relaxation (206). A follow-up study proved that these chromophores could be used for photoacoustic lifetime imaging of hypoxia *in vivo* in tumor-bearing mice (207). In summary, photoacoustic imaging is one of the youngest members of the molecular imaging community. It is foreseen as a future noninvasive clinical tool for accurate detection and characterization of, for example, carotid plaques in patients (201) and is characterized by an exceptional improved imaging depth compared to optical imaging. Furthermore, photoacoustic imaging can be easily combined with traditional ultrasound, which will provide anatomic, functional, and molecular information with a single image (15).

4. BIORESPONSIVE MRI PROBES: ACTIVATION OF THE MRI CONTRAST AGENT

In contrast to optical imaging, MRI can be employed for whole-body diagnostic imaging in humans. MRI presents an attractive platform for molecular imaging due to the conjunction of high-resolution anatomical imaging and mapping of the activity of specific biomarkers by MRI contrast agents. Unlike optical or radiolabeled molecular imaging probes, MRI contrast agents, such as gadolinium chelates, do not directly generate a signal but are detected through their ability to shorten the water proton relaxation times, that is, the longitudinal (spin–lattice) and transverse (spin–spin) relaxation times (T_1 and T_2,

respectively) (208). In a T_1-weighted MRI image, T_1-shortening results in positive contrast (bright spots), whereas in a T_2-weighted image, T_2-shortening generates negative contrast (dark areas). The longitudinal relaxivity (r_1) of a contrast agent is modulated by several parameters (209,210), including the number of inner sphere water molecules directly coordinated to paramagnetic complex (q), τ_m the exchange rate of the metal-coordinated water molecule with the bulk water, and τ_R the rotational correlation time of the contrast agent (Fig. 8). Smart MRI contrast agents have been developed that show a change in one of these parameters upon activation due to a biochemical stimulus leading typically to an increase in r_1. Typically, these MRI contrast agents go from an "off" state, with a minimal effect on T_1/T_2, to an "on" state, with a large effect on T_1/T_2 shortening (17,210,211). In the next paragraphs, we will present an overview of MRI imaging probes that generate a change in contrast as a result of activation of the MRI contrast agent. Interestingly, during the preparation of this manuscript, an in-depth review specifically focussed on responsive MRI probes has been reported (212).

4.1. Bioresponsive T_1-weighted MRI contrast agents

4.1.1. Longitudinal relaxivity enhancement via modulation of water coordination sites

Several strategies have been explored to enhance the longitudinal relaxivity of paramagnetic gadolinium complexes after its activation due to an increase in the number of water molecules directly coordinated to the metal centre (Scheme 4). The first enzymatic activatable agent has been reported by Meade and coworkers (213,214), in which the water coordination site of gadolinium complex was blocked with a galactopyranosyl ring reducing "q" ($q << 1$). Its enzymatic cleavage by the reporter enzyme β-galactosidase restores the water coordination site ($q = 1$) leading to an efficient T_1-shortening. Another class of gadolinium-based agents can interact with endogenous metal ions, such as Ca^{2+} and Zn^{2+}, resulting in an increase in water coordination sites and thus improved longitudinal relaxivity (215,216). A third class of activatable MRI contrast agents uses pH-responsive gadolinium chelates that display relaxation enhancement at acidic conditions (217–219). Finally, a recent class

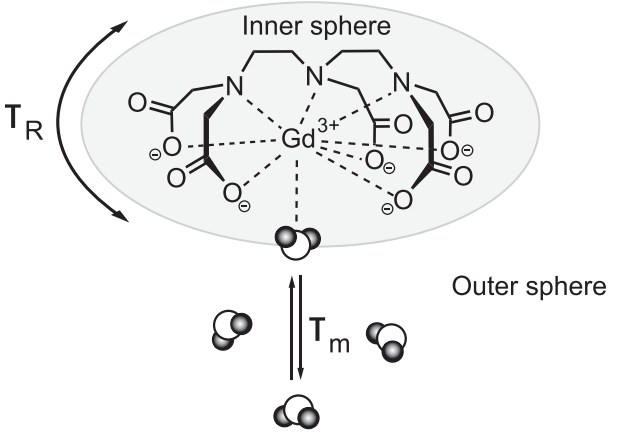

Figure 8. Schematic representation of the most relevant parameters that influence the relaxation of a gadolinium-DTPA-based MRI contrast agent: the rotational correlation time (τ_R) and the mean residence time of the water molecules at the inner sphere (τ_m).

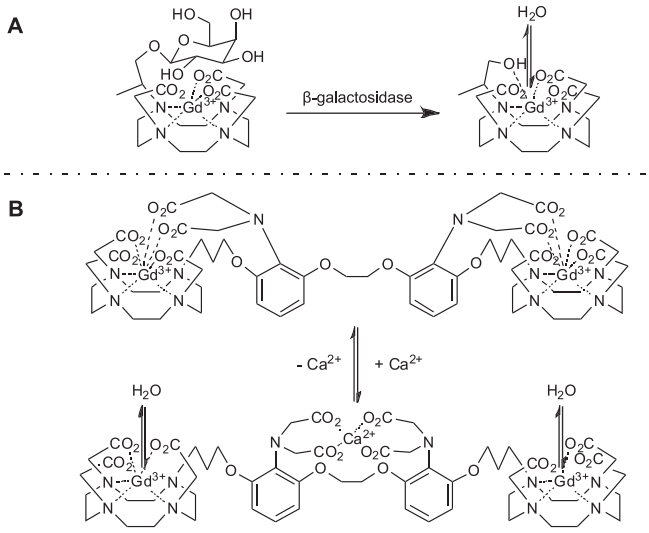

Scheme 4. Gd^{3+}-based MRI contrast agents displaying an increase in water coordination sites upon activation, and thus enhanced longitudinal relaxivity. (A) Enzymatic activation of a galactopyranosyl-masked Gd^{3+}-DOTA by β-galactosidase (214). (B) Activation of an MRI contrast agent by a conformational change upon Ca^{2+} target binding Y.

used redox responsive gadolinium chelates, for which q does increase upon reaction with NADH (220). Despite the development of various bioresponsive MR imaging probes of this class (213–220), exploration *in vivo* has been limited (221). A cell-permeable Zn^{2+} sensing MR imaging probe showed the detection of elevated Zn^{2+} levels in the hippocampus in rats (221). Importantly, intracranial injection of the imaging probe was performed to obtain sufficient imaging probe concentration in the brain. Typically, the exogenous imaging probe concentration at the target site should be >1 uM because of the relatively low sensitivity of MRI, which requires relative high biomarker concentrations (212). Furthermore, there is a need for efficient cellular transport of most of these agents to reach their intracellular targets. Therefore, to apply these probes *in vivo* may be challenging, especially in case of intravenous injection, and may limit clinical translation.

Reducing the water mobility can modulate changes in the longitudinal relaxivity of the protons of water molecules. For example, pH-sensitive micelles and liposomes have been reported containing gadolinium-based complexes in its aqueous lumen (222–224), which have a low effect on the longitudinal relaxivity of the protons of the bulk water molecules due to the limited transmembrane water exchange rate. At low pH, the contrast agents are released and a strong increase in the longitudinal relaxivity is observed. In another approach, gadolinium chelates were efficiently quenched by encapsulation in the polymer coating of a superparamagnetic iron oxide particle (225). In acidic environments the Gd chelates were efficiently released with a subsequent increase in longitudinal relaxation rate.

4.1.2. Relaxivity enhancement via modulation of rotational correlation time

T_1-shortening of the protons of water molecules can be achieved by slowing down the molecular tumbling rate of the paramagnetic complex ($1/\tau_R$) (226). Nivorozhkin and coworkers have developed a carboxypeptidase B activatable MRI contrast agent that gained affinity for the high molecular weight

protein albumin upon activation, resulting in a reduced tumbling rate and therefore higher relaxivity (227). In similar approaches, activatable albumin/protein-binding Gd-based MRI contrast agents have been developed for the detection of reporter enzyme β-galactosidase, carbonic anhydrase, and zinc *in vitro* (228–231). In another approach, Gd-based MRI contrast agents showed polymerization upon specific activation by myeloperoxidase (MPO), resulting in a slower tumbling rate and therefore in an enhancement of the longitudinal relaxivity (232–236) (Fig. 9). In this approach, Gd-labeled phenol derivatives are oxidized by MPO, resulting in tyrosyl radicals, which will form dityrosine cross-links. Using this approach, MPO activity was visualized in a mouse model of myocardial infarction *in vivo* (233).

4.2. Bioresponsive T_2–weighted MRI contrast agents

Superparamagnetic iron oxide (SPIO) nanoparticles are widely used as T_2-weighted MRI contrast agents. Recently, it has been shown that clusters of SPIOs display faster T_2 relaxation properties of the individual iron oxide cores compared to the non-clustered iron oxide cores. Furthermore, clustering results in an increased concentration of the MRI contrast agent and, therefore, both processes contribute to an enhanced transverse relaxivity (237). Activatable SPIOs have been developed that cluster upon activation by MPO. In this approach, dopamine was attached to the surface of the SPIOs. In the presence of MPO and H_2O_2, this phenol derivative is transformed into a tyrosyl radical that causes dityrosine cross-links between the nanoparticles (238). In another strategy, biotin and neutravidin coated SPIOs were shielded with polyethylene glycol (PEG) that could be proteolytically removed by MMP-2 to initiate self-assembly (239,240) (Fig. 10). In a related approach, Schellenberger *et al*. designed iron oxide particles sterically stabilized by PEG that showed significant aggregation by interparticle electrostatic and magnetic attraction upon MMP-9-induced dePEGylation (241). Finally, Atanasijevic *et al*. reported on SPIOs that were functionalized with calmodulin, a Ca^{2+} sensing protein, and showed Ca^{2+}-dependent protein–protein interaction driving particle clustering (242).

In contrast to the clustering of SPIOs, several iron-oxide-based imaging probes have been developed that show disassembly upon probe activation, resulting in a loss of relaxivity enhancement. In these disassembly approaches the individual iron oxide particles are connected to each other by cleavable linkers. Following this strategy, probes has been developed for the sensing of caspase-3, MMP-2, and endonucleases *in vitro* in experimental settings (243–245). The fact that enzyme activation results in loss of relaxivity enhancement challenges applications of this approach for imaging *in vivo*.

In another strategy (246), iron oxides were encapsulated in a polymer coating restricting the interaction of the iron oxide core with surrounding water. *In vitro* enzymatic degradation of the dextran coating by dextranase resulted in a strong T_2 shortening.

4.3. Bioresponsive paramagnetic CEST MRI agents

Another class of activatable paramagnetic MRI contrast agents induces MR contrast enhancement utilizing chemical exchange saturation transfer (CEST) (17,247). Typically, these CEST MRI contrast agents consist of lanthamide complexes containing exchangeable water protons with a large chemical shift compared to the bulk water protons. Upon irradiation of these exchangeable water protons using a selective radiofrequency pulse, the intensity of the bulk water signal is reduced via chemical exchange saturation transfer. Bioresponsive paramagnetic CEST agents have been designed that display a change in the CEST effect upon interaction with a biochemical stimulus (17,247). For instance, Pagel and coworkers reported on a paramagnetic CEST agent that showed urokinase plasminogen activator (uPA) specific degradation, whereby an amide was cleaved and transformed into an amine, which caused disappearance of CEST (248) (Fig. 11). In another approach, a redox sensitive CEST agent was developed that could switch between paramagnetic Co(II)

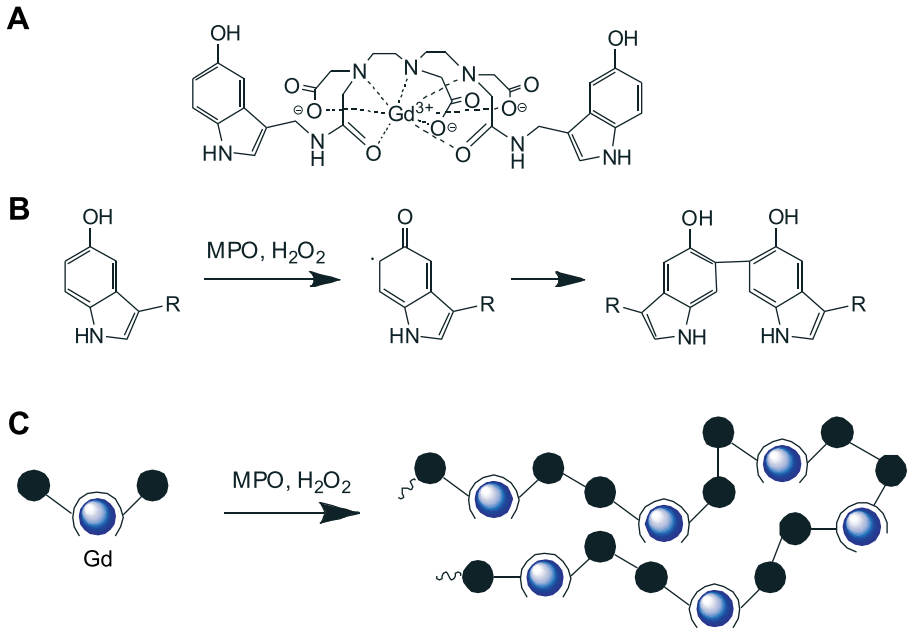

Figure 9. (A) Chemical structure of a MPO polymerizable Gd^{3+}-DTPA-based MRI contrast agent (232). (B,C) Mechanism of MPO catalyzed polymerization resulting in an increased local concentration of the MRI contrast agent Gd^{3+} and enhanced T_1-relaxivity.

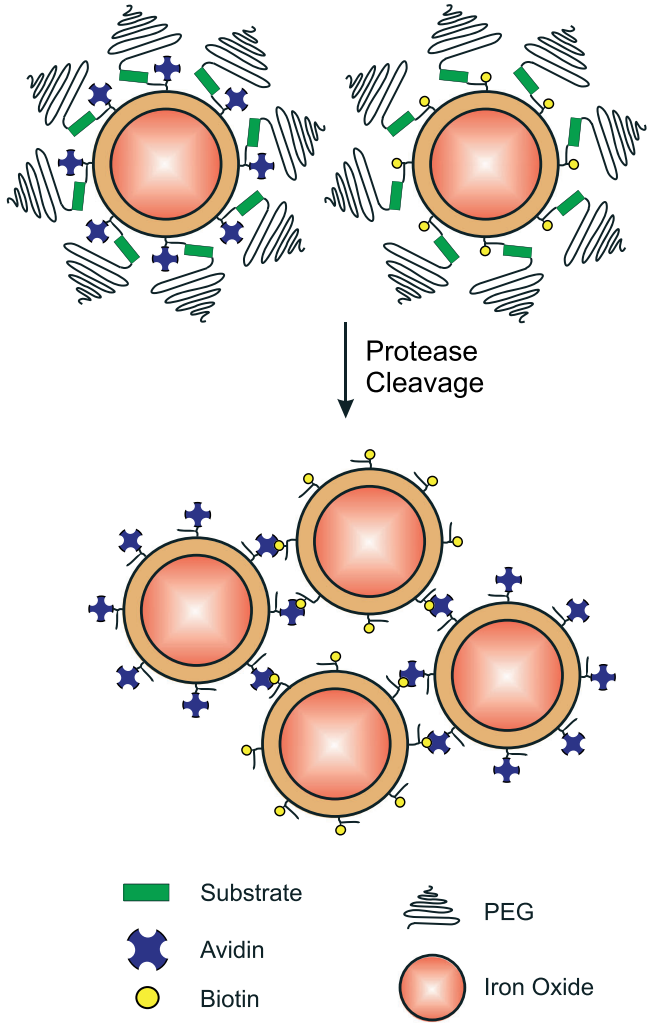

Figure 10. Mechanism of proteolytic actuation of iron oxide self-assembly. Avidin- and biotin functionalized iron oxide nanoparticles are shielded by PEG chains. Upon proteolytic removal of PEG, biotin and neutravidin particles self-assemble into clusters, resulting in an enhanced transverse relaxivity.

with a high CEST signal to a diamagnetic Co(III) state with a low CEST signal (249). Oxidation of the CEST agent resulted in Co(III) and a reduction in CEST signal, as was demonstrated *in vitro* (249). Various other bioresponsive CEST agents have been developed to monitor pH differences, redox status, ROS, metabolites, enzymes, and minerals (250–262). Most of these probes have been limited to validation *in vitro*, while studies *in vivo* are needed to reveal potential clinical translation. A particular challenge may be to obtain sufficient concentration of imaging probes at the target site, especially in the case of intracellular targets. Importantly, two recent papers have explored the use of bioresponsive CEST agents *in vivo* (248,263). First, an uPA sensitive CEST agent, which showed disappearance of CEST upon activation, was used to detect uPA in tumor-bearing mice (248). The other preclinical study was performed with a hypoxia-sensitive CEST agent (263). This CEST agent contained two paramagnetic nitroxide free radical groups that quenched the CEST signal due to rapid T_1 relaxation of water by the nitroxide unpaired electrons. Upon reduction to *bis*(hydroxylamine) in hypoxic areas, the T_1 relaxation is restored and the CEST signal is activated. Reduction of this probe *in vivo* was successfully detected and warrants further research in preclinical models of disease (263).

A general drawback for all the above activatable MRI contrast agents is the need for a pre- and post-MRI scan to calculate contrast changes by subtraction of the two images, which requires strict image registration to prevent any artefact. This is especially challenging if probe activation takes time and one scan session is not enough. Furthermore, any morphological changes between scans (e.g. tumor shrinkage due to therapy) strongly hampers correct image subtraction and final interpretation.

4.4. Bioresponsive hyperpolarized MR agents

A final class of activatable MR contrast agents are hyperpolarized probes useful for imaging of metabolic pathways (264). Hyperpolarization of the probe results in a significant redistribution of the populations of nuclear spins in a magnetic field, leading to a signal increase by a factor of 10,000 or more. Whereas the concentration of endogenous metabolites is below the detection threshold of MRI, hyperpolarized metabolic molecules can be detected and are widely used to study changes in cancer-associated metabolic pathways (264). Importantly, the relaxation of the hyperpolarized agents will be determined by the T_1 relaxation time. For that reason, typical long-life T_1 atoms such as ^{13}C (>20 s half-life) are best-suited for this technology. Multipe ^{13}C metabolic agents have been developed and investigated *in vitro* and/or *in vivo*, such as ^{13}C-hyperpolarized lactate, pyruvate, fructose, and glutamine (264–266). For example, hyperpolarized [5-^{13}C]glutamine was used to study glutaminase activity *in vivo* in liver cancer metabolism in rats (265). Very recently, a first study in a human was successfully performed with hyperpolarized [1-^{13}C]pyruvate to characterize tumor metabolism in prostate cancer, indicating that clinical translation of this technology is feasible (266).

5. BIORESPONSIVE PROBES FACILITATING SITE-SPECIFIC RETENTION OF THE IMAGING LABEL

Activation of autoquenched, self-quenched, and FRET optical probes results in the transition of a fluorophore from an "off" state to an "on" state or FRET between a donor and acceptor fluorophore. For the imaging probes that are activated by extracellular proteases, for example MMPs, the fluorophores may diffuse away from the cleavage site, resulting in lower signal-to-background ratios (267). Similarly, activatable MRI contrast agents might show wash-out after activation, except for the activatable SPIOs. In order to avoid wash-out, a special class of activatable probes has been developed in which the fluorescent or MRI imaging label is not activated, but probe activation leads to retention of the imaging probe at the activation site, thereby accumulating the imaging label in the target tissue and thus increasing signal. Importantly, these types of imaging probes are not limited to one specific imaging modality. Therefore, this approach led to the successful development of bioresponsive nuclear imaging probes. In the following paragraphs the different approaches to achieve specific retention of the imaging label will be addressed. First, probes will be discussed that require the presence of a specific target for activation and are not amendable to the detection of other targets. Thereafter, activatable

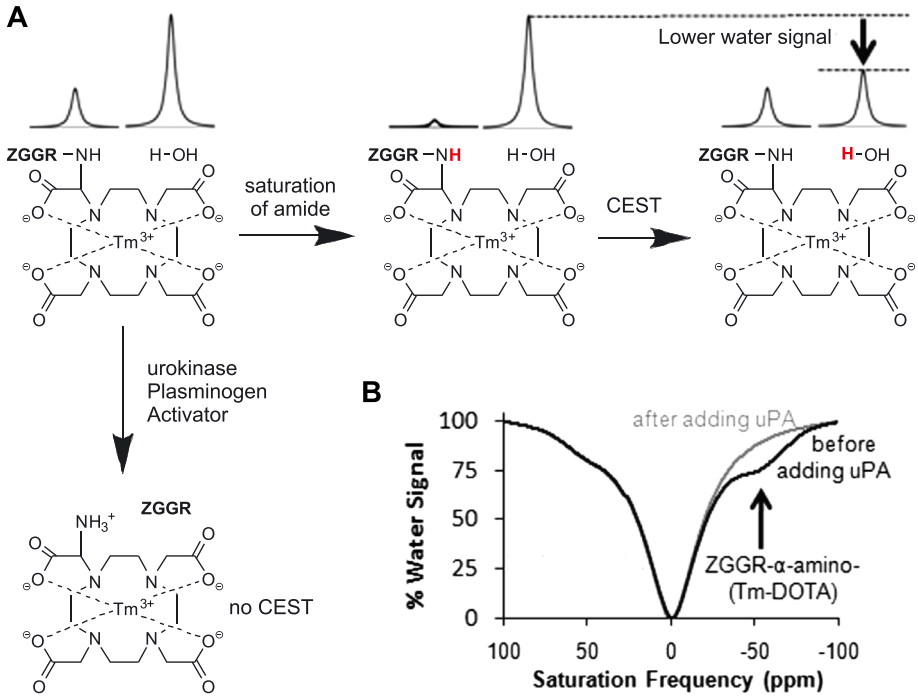

Figure 11. (A) Mechanism of an uPA sensitive CEST agent (248). The horizontal reaction shows MR saturation of the amide proton (in red), followed by CEST, which transfers the MR saturation to water and decreases the water signal. The vertical reaction shows cleavage of the ZGGR peptide by uPA, which results in the conversion of the amide to an amine that does not generate CEST. (B) The uPA sensitive CEST probe showed CEST in the absence of uPA but not after cleavage by uPA. Figure is reprinted (adapted) with permission from (248).

molecular imaging probes will be discussed where retention can be modulated by a wider variety of targets by including different substrates/triggers.

5.1. Bioresponsive accumulating probes lacking tuning possibilities for novel targets

In this section, activatable imaging probes will be discussed that show retention and accumulation of the imaging label upon activation. All these probes are designed to be specifically activated by a unique biomarker (e.g. specific enzyme, pH, hypoxic tissue) and typically lack the possibility to be adapted to a wide variety of targets.

5.1.1. Bioresponsive accumulating probes restricted to specific enzymes

An example of an activatable imaging probe that has a narrow target-application range has been developed by the group of Ruoslahti (268,269). In their work, fluorescent probes have been developed that specifically penetrate integrin and neuropilin overexpressing cells upon proteolytic activation. These probes were successfully targeted to tumors through a three-step process: first an RGD-peptide motif mediated binding to integrins on tumor endothelium. Subsequent proteolytic degradation of the probe exposed a C-terminal R/KXXR/K motif, which mediated neuropilin-1-dependent cellular penetration (269).

In another approach, fluorescent, MRI, and radiolabeled probe analogs were developed displaying specific cross-linking to thrombi by the activity of transglutaminase FXIIIa (270–274). In a mouse model of myocardial infarction, transglutaminase FXIIIa activity was successfully detected using a radiolabeled analog (273,274). Redesigning this probe to achieve cross-linking upon interaction with other enzymatic targets, such as MMPs, that do not show transglutaminase activity is cumbersome. Therefore this type of imaging probe cannot be adapted to detect a wide range of other targets. Recently, another MRI activatable probe was developed that upon activation binds efficiently to fibrin in fresh thrombi (275). The probe is based on a low-affinity fibrin-binding linear peptide that becomes cyclic by the activity of protein disulfide isomerase. Upon cyclization of the imaging probe, the probe showed strongly enhanced fibrin binding. Because protein disulfide isomerase is only present on activated platelets the activated MRI imaging probe predominantly bound to fresh thrombi *in vitro*. Furthermore, a metalloporphyrin MRI imaging probe was developed that became insoluble after cleavage of phosphate end-groups by the reporter enzyme secreted alkaline phosphatase (276). This probe showed strong accumulation and T_1 shortening *in vivo* in the vicinity of the areas expressing the reporter enzyme.

Intracellular enzymatic targets have been successfully targeted with radiolabeled probes showing increased retention upon enzymatic activation. Intensive research over many decades has resulted in various ^{18}F activatable PET probes that are intracellularly phosphorylated and subsequently trapped. A well-known example is the clinically applied PET imaging probe ^{18}F-fluorodeoxyglucose (FDG) that is used for imaging of glucose metabolism (277). Cancerous tissue typically has a high metabolic activity characterized by an increased uptake of glucose/FDG. Subsequently, the elevated intracellular activity of the enzyme hexokinase enables efficient phosphorylation of FDG, resulting in cellular entrapment and subsequent accumulation of the radiolabeled probe (Scheme 5) as further downstream probe metabolism is blocked. Other phosphorylation sensitive PET imaging probes have been developed for the imaging of cell proliferation: ^{18}F-fluoro-3′-deoxy-3′-L-fluorothymidine (FLT) and

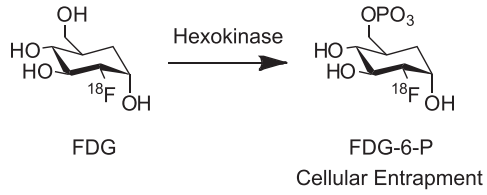

Scheme 5. Phosphorylation of FDG.

^{18}F-choline (278–280). FLT is a thymidine analog that is incorporated into the DNA of proliferative cells, such as those found in tumor tissue. Once FLT is taken up by cells and phosphorylated by thymidine kinase 1, it becomes trapped intracellularly (278). ^{18}F-choline is incorporated in the membrane of cancer cells that show increased lipid synthesis during tumor cell growth (279,280). Specifically, choline is phosphorylated by choline kinase and subsequently built into the cell membrane as phosphatidylcholine. Both FLT and ^{18}F-choline are clinically used for imaging of different types of proliferating cancers in patients (280,281). Recently, an advanced H_2O_2 activatable FLT probe was developed for ROS detection in proliferative cells (282). Validation of this probe *in vivo* is expected and such a probe may be valuable for detection of ROS-producing cancers. Another paper described a dual-strategy for imaging of secondary Cerenkov induced fluorescence using both FDG and an MMP-sensitive fluorescein-quencher optical probe (283). Local FDG nuclear radiation will result in Cerenkov radiation, which can be absorbed by the fluorescein-containing optical probe. In case fluorescein is activated and released by MMP, absorption of Cerenkov radiation will result in a fluorescent signal. It was demonstrated that this probe can detect concomitant enzyme and glycolytic activity *in vivo* (283). Another intracellular target that can phosphorylate radiolabeled probes, leading to cellular probe accumulation, is herpes simplex virus-1 thymidine kinase (284). In this approach, a probe, for example FIAU (1-(2′-deoxy-2′-fluoro-1-β-D-arabinofuranosyl)-5-iodouracil is used, which resembles the nucleotide uridine. In contrast to mammalian thymidine kinase, the herpex simplex virus-1 thymidine kinase (HSV1-TK) is less discriminative and is able to phosphorylate these probes, leading to trapping and accumulation in cells expressing HSV1-TK. This enzyme is extensively used in reporter gene imaging approaches using PET or SPECT as a research tool (284,285), but has also clinically been tested in glioma imaging (286) as well as in combination with ganciclovir in enzyme/prodrug therapy of gliomas (287). Zhang *et al*. developed a FRET imaging probe for the detection of Bruton's tyrosine kinase in live cells (288). Reaction of the imaging probe with kinase resulted in removal and cellular washout of the quencher and activation and retention of the optical imaging label.

Next to kinases, other intracellular enzymes such as caspases, indicative for apoptosis, have been targeted with activatable imaging probes resulting in enhanced retention. For example, radiolabeled cell-penetrating caspase substrates were developed for SPECT imaging and showed enhanced retention in apoptotic cells *in vitro* (289) and in tumors *in vivo* (290).

Finally, dynamic changes in glycosylation, the posttranslational modification of proteins, are associated with tumor progression (291). Therefore, imaging strategies have been explored to image tissue glycosylation *in vivo* (292,293). In these strategies, bioresponsive sugar analogues containing a bioorthogonal functional group (e.g. azide) are metabolized and incorporated into cell-surface glycans. The azide can subsequently react with imaging probes bearing a complementary bioorthogonal functional group. This technique was demonstrated in zebrafish (294), but translation to rodents to specifically visualize tumor tissue has proven challenging, as the azidosugars are metabolized and incorporated into glycans in various tissues (291). Therefore, Xie *et al*. employed targeted liposomes to deliver the bioresponsive azidosugars specifically to the tumor tissue. Tumor glycan-specific incorporation of the azidosugars *in vivo* was demonstrated using a bioorthogonal optical imaging probe (291).

5.1.2. *Bioresponsive probes accumulating in acidic tissues*

Differences in pH between diseased and healthy tissue have been used to mediate the retention of imaging probes in diseased tissues. For example, an electrostatically quenched cell-penetrating micelle was selectively activated at the lower extracellular pH of the tumor microenvironment (on average pH is between 6 and 7 (130)), resulting in intracellular accumulation and release of a model drug (295). This model system may also be used to release and activate optical imaging probes (Fig. 12). An alternative approach is aimed at the local

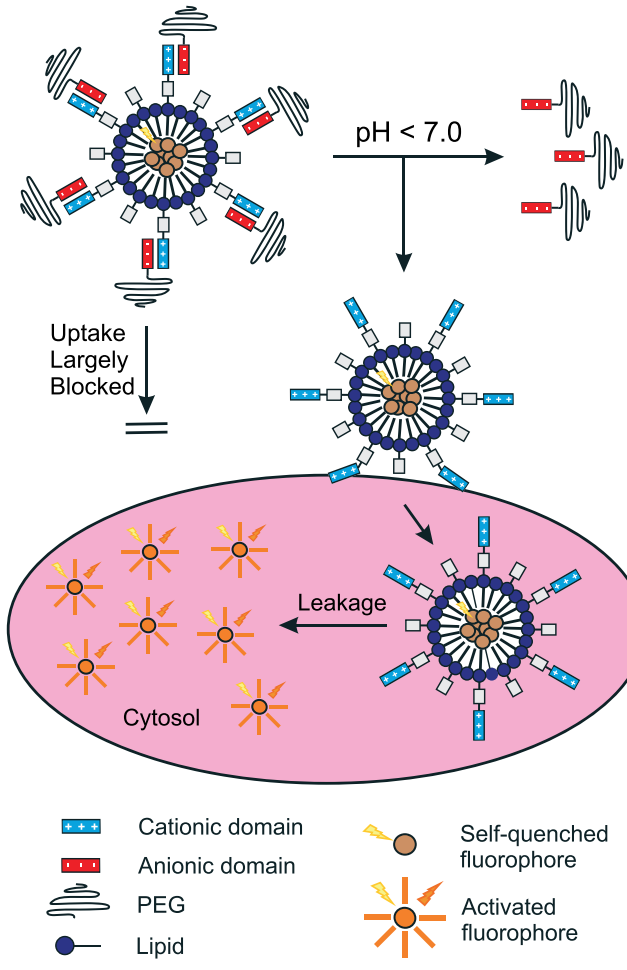

Figure 12. Mechanism of a pH-dependent cell-penetrating micelle. The cell-penetrating property of polycationic peptide functionalized micelles is masked by polyanionic polymers. At pH < 7.0 dissociation will take place, leading to cellular uptake of the micelle. Subsequent leakage of the fluorophores will result in restoration of fluorescence.

release and accumulation of iron-oxide particles from pH-responsive polymeric micelles at acidic conditions (296). This activatable T_2 MRI contrast agent was used for the detection of ischemic areas in the brain of rats. Furthermore, pH-dependent cell-membrane insertion peptides containing either a fluorescent or a radioactive imaging label were developed and showed efficient membrane tagging and specific retention in acidic tumor tissues (297,298).

5.1.3. *Bioresponsive probes accumulating in hypoxic tissues*

Over the past decades, much research has been devoted to the development of imaging probes for detection of hypoxic areas, often encountered in tumors that grow beyond the region reached by vascular oxygen (299,300). The first probes were based on radiolabeled 2-nitroimidazoles. After cellular entry via diffusion, the 2-nitroimidazole moiety undergoes an enzyme-mediated single-electron reduction to produce reactive oxygen radical anions. In normoxic tissues, the radical anion is rapidly back-oxidized to the original compound and eventually diffuses out of the cells and tissues. In hypoxic tissues, however, the radical anion may be further reduced and subsequently will be trapped in cells via covalent binding to the macromolecular components (301). A PET imaging probe, ^{18}F-fluoromisonidazole (FMISO), has been administered in patients and demonstrated to be a valuable tool for the evaluation of tumor response during and after fractionated radiation therapy (302). Second- and third-generation 2-nitroimidazole probes (^{18}F-fluoroazomycin arabinoside (FAZA) and ^{18}F-flortanidazole (HX4)) have also shown promising *in vivo* results in patients with head and neck cancer (303–305). Another well-studied probe is ^{64}Cu-diacetyl-*bis*(N^4-methylthiosemicarbazonate), Cu-ATSM. Upon cellular uptake, Cu(II)-ATSM is reduced to an unstable Cu(I)-ATSM probe, followed by dissociation of the metal complex and subsequent irreversible trapping of Cu(I) within the cell (306). While other processes such as copper metabolism may play a role in Cu-ATSM tumor uptake, this probe showed clinical value for patient diagnostics (299,306,307). Furthermore, other hypoxic imaging probes have recently been developed. A 4-nitrobenzylester-containing ^{99m}Tc-probe showed efficient reduction to a cell-membrane impermeable carboxylate anion with consequent cellular retention *in vitro* (308). Finally, a radiolabeled-peptide-based probe was developed that was degraded and retained in hypoxia-inducible factor-1 active tumor regions *in vivo* (309).

5.2. Bioresponsive accumulating probes enabling tuning for target specificity

In this section, bioresponsive accumulating molecular imaging probes will be discussed that can be applied for the detection of a wide variety of targets. A first class of probes exhibit hydrophobic clustering upon proteolytic removal of a hydrophilic component, thereby decreasing the *in vivo* clearance rate from the target tissue (310–312) (Fig. 13). These probes showed good promise for the detection of MMP-2 and MMP-7 *in vivo*, employing MRI T_1-contrast agents as imaging labels (310–312). Recently, this concept was further developed for PET purposes. Hereto, an ^{18}F-labeled hydrophobic tetramethylrhodamine moiety was conjugated to a hydrophilic PEG linker by an MMP-2 cleavable substrate (313).

A second imaging concept was proposed by Tsien and coworkers. They reported on activatable cell-penetrating peptide (ACPP) imaging probes functionalized with fluorophores or MRI contrast agents (314–319) (Fig. 14A). These constructs consisted of an MMP-2/9 substrate inserted in between a polyanionic peptide and a polycationic cell-penetrating peptide (CPP) conjugated to the imaging probe. The cell-penetrating property of the polycationic peptide was neutralized due to intramolecular electrostatic interactions with the polyanionic domain, preventing cellular uptake of the probe. Cleavage of the substrate by tumoral MMP-2/9 released the polycationic from the polyanionic domain, thereby triggering cellular adhesion and subsequent uptake of the imaging label-functionalized polycationic peptide in tumors. A threefold higher tumor uptake was observed for MMP-2/9 ACPP compared to a scrambled negative control (314). However, it was recently demonstrated that the tumor targeting of a radiolabeled MMP-2/9 sensitive ACPP

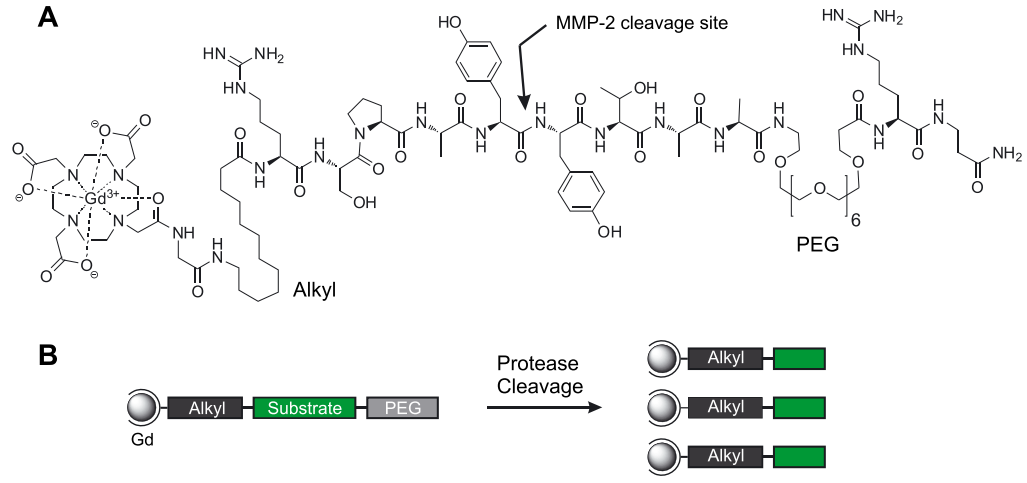

Figure 13. (A) Chemical structure of a MMP-2 activatable solubility switchable MRI T_1-contrast agent (310). A Gd^{3+}-DOTA functionalized hydrophobic alkyl chain is conjugated to a hydrophilic PEG chain via an MMP-2 cleavable peptide substrate (RSPAY-YTAA). (B) Schematic representation; upon proteolytic removal of the hydrophilic PEG chain, the alkyl chain will provide a decrease in solubility, resulting in tissue retention of the Gd-labeled domain at the target site and subsequent enhanced T_1-relaxivity.

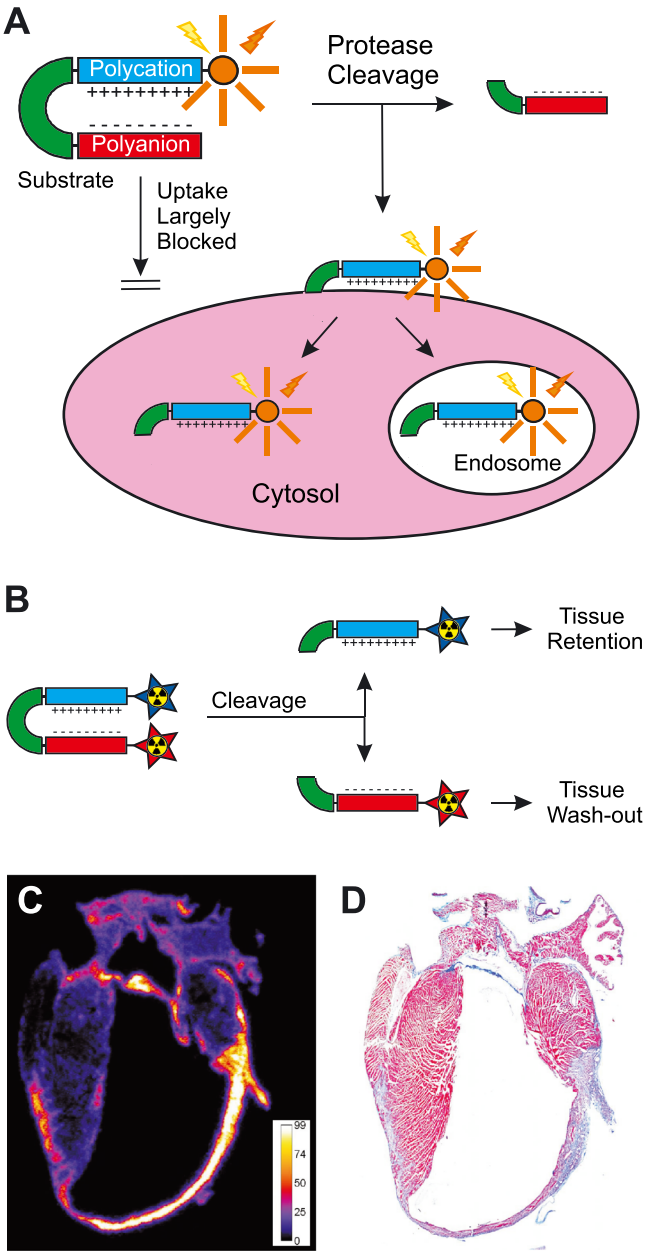

Figure 14. (A) Mechanism of a fluorescently labeled protease activatable cell-penetrating peptide (ACPP). The cell-penetrating property of a polycationic peptide is masked by a polyanionic peptide. Proteolytic degradation of the linker releases the polycationic cell-penetrating peptide, which will transfer the fluorophore label across the cell membrane. (B) Mechanism of a dual-isotope radiolabeled protease activatable cell-penetrating peptide. Proteolytic degradation of the linker releases the polycationic cell-penetrating peptide, which will transfer its radionuclide cargo (in blue) across the cell membrane. The polyanionic peptide and its radionuclide cargo (in red) will be cleared from the target tissue. The ratio of the radionuclide cargoes (blue-over-red) is a measure for local ACPP activation. (C) Imaging of MMP-activity in post-ischemic cardiac remodeling using an MMP-2/9 sensitive radiolabeled ACPP. (D) Azan staining of an adjacent coronal section showing the infarct scar in blue and remote myocardium in red. Figure C and D are reprinted with permission from van Duijnhoven *et al.* (323). Copyright 2014 American Chemical Society.

is most likely not caused by tumor-specific activation but due to activation of ACPP in the vasculature and subsequent elevated uptake in the tumor due to its enhanced permeability (320,321). In this work, dual-isotope radiolabeled ACPPs have been designed that allow *in vivo* discrimination between uptake of the activated probe and the integral probe (Fig. 14B). Most likely, tumor-specific ACPP activation have been limited due to low absolute tumoral MMP activity as a result of local MMP inhibition by the family of tissue inhibitors of metalloproteinases (TIMPs) (321,322). In a cardiovascular-disease-related mouse model, a dual-isotope radiolabeled MMP-2/9 sensitive ACPP probe was successfully employed to detect MMP activity in the context of post-ischemic myocardial remodeling (323) (Fig. 14C and D). Furthermore, a ratiometric Cy5/Cy7 labeled MMP-2/9 sensitive ACPP probe allowed the real-time detection of MMP activity in a murine asthma model (324).

The ACPP imaging concept was further explored for the detection of disease-related enzymes such as urokinase, enterokinase, MMP-14, and plasmin *in vitro* (314,325–327), as well as acidic conditions, by employing a reduction-sensitive disulfide bridge between the polycationic and polyanionic domain (314). A novel tumor-homing ACPP, predominantly sensitive for elastases, was identified by a parallel *in vitro* and *in vivo* selection with phage displaying a library of ACPPs (328). Introduction of a NIR quencher at the polyanionic domain led to development of MMP-2 and MMP-7 FRET-based ACPP imaging probes that showed both *in vitro* activation of fluorescence as well as cellular retention upon cleavage (202,329). Furthermore, the similar MMP-2 ACPP probe was succesfully employed in photoacoustic imaging of MMPs in thyroid carcinomas *in vivo* (203). Recently, progress was made in the development and application of ratiometric ACPP imaging probes for *in vivo* detection of thrombin (330,331) and H_2O_2 (167). Finally, it was shown that cellular uptake of ACPP functionalized nanocarriers *in vitro*, that is, MRI contrast agent functionalized dendrimers (317) or quantum dots (332), could be modulated by MMP-2. MMP-induced cellular uptake of quantum dots *in vitro* was also achieved by dePEGylation of CPP functionalized quantum dots (333).

Recently, a new class of activatable oligomerizable imaging probes has been developed. These probes contain both a N-terminal cysteine residue and a 6-amino-CBT group, in which the former group is protected by a protease-sensitive substrate. Removal of the substrate will liberate the N-terminal D-cysteine residue, allowing an intermolecular condensation reaction between D-cysteine and 6-amino-CBT, yielding a linear oligomer that accumulates. This strategy has been successfully employed to detect intracellular furin by optical and photoacoustic imaging (334,335) and might be applicable to other intracellular proteases that yield an N-terminal cysteine upon cleavage.

In another approach, cell-internalization was achieved upon activation of a lipid-containing FRET probe (336). This probe was targeted to the plasma membrane and activation of the probe by MMP-12 resulted in efficient internalization and retention of the donor fluorophore.

Finally, bioresponsive accumulating probes have been developed that need a second target for site-specific retention after its initial activitation. For example, protease-activatable probes have been designed to result in specific retention of the imaging label by tagging of an MMP-2/14 activated transmembrane domain to the cell membrane (337) or specific internalization of an MMP-9 activated probe into scavenger receptor class A type

I expressing macrophages (338). Another example is a fluorescent probe that showed enhanced binding to collagen fibers upon proteolytic activation *in vitro* (339,340).

6. CONCLUDING REMARKS

In summary, this review highlights the state-of-the-art of the design and potential application of bioresponsive molecular imaging probes for the monitoring of endogenous targets *in vivo*. Various strategies of bioresponsive imaging probes have been discussed, varying from protease activatable probes for which the molecular target can continuously activate the imaging probe to a broad spectrum of other endogenous targets for which the imaging label either undergoes a transition from an "off" to an "on" state or is specifically retained at the site of activation. Current and novel bioresponsive molecular imaging probes may play a pivotal role in gathering molecular information underlying biological and cellular processes in basic biology and disease. Therefore, we strongly believe that bioresponsive probes will find various clinical applications, including in (i) diagnostics to improve accurate detection of disease, (ii) intraoperative imaging-guided surgery to improve tumor margin detection, and (iii) real-time assessment of efficacy of therapy/surgery.

REFERENCES

1. Mankoff DA. A definition of molecular imaging. J Nucl Med 2007; 48: 18N–21N.
2. Hoffman JM, Gambhir SS. Molecular imaging: The vision and opportunity for radiology in the future. Radiology 2007; 244: 39–47. doi:10.1148/radiol.2441060773.
3. Massoud TF, Gambhir SS. Integrating noninvasive molecular imaging into molecular medicine: An evolving paradigm. Trends Mol Med 2007; 13: 183–191. doi:10.1016/j.molmed.2007.03.003.
4. Weissleder R, Pittet MJ. Imaging in the era of molecular oncology. Nature 2008; 452: 580–589. doi:10.1038/nature06917.
5. Pysz MA, Gambhir SS, Willmann JK. Molecular imaging: Current status and emerging strategies. Clin Radiol 2010; 65: 500–516. doi:10.1016/j.crad.2010.03.011.
6. Contag CH. *In vivo* pathology: Seeing with molecular specificity and cellular resolution in the living body. Annu Rev Pathol 2007; 2: 277–305. doi:10.1146/annurev.pathol.2.010506.091930.
7. Willmann JK, Bruggen NV, Dinkelborg LM, Gambhir SS. Molecular imaging in drug development. Nat Rev Drug Discov 2008; 7: 591–607. doi:10.1038/nrd2290.
8. Herschman HR. Molecular imaging: Looking at problems, seeing solutions. Science 2003; 302: 605–608. doi:10.1126/science.1090585.
9. Lammers T, Kiessling F, Hennink WE, Storm G. Nanotheranostics and image-guided drug delivery: Current concepts and future directions. Mol Pharmaceutics 2010; 7: 1899–1912. doi:10.1021/mp100228v.
10. Ntziachristos V, Yoo JS, van Dam GM. Current concepts and future perspectives on surgical optical imaging in cancer. J Biomed Opt 2010; 15: 066024; doi: 10.1117/1.3523364
11. Urano Y, Sakabe M, Kosaka N, Ogawa M, Mitsunaga M, Asanuma D, Kamiya M, Young MR, Nagano T, Choyke PL, Kobayashi H. Rapid cancer detection by topically spraying a γ-glutamyltranspeptidase-activated fluorescent probe. Sci Transl Med 2011; 3: 110ra119; doi: 10.1126/scitranslmed.3002823
12. Frangioni JV. New technologies for human cancer imaging. J Clin Oncol 2008; 26: 4012–4021. doi:10.1200/JCO.2007.14.3065.
13. Van de Wiele C, Oltenfreiter R. Imaging probes targeting matrix metalloproteinases. Cancer Biother Radiopharm 2006; 21: 409–417. doi:10.1089/cbr.2006.21.409.
14. Razgulin A, Ma N, Rao J. Strategies for *in vivo* imaging of enzyme activity: An overview and recent advances. Chem Soc Rev 2011; 40: 4186–4216. doi:10.1039/C1CS15035A.
15. Wilson KE, Wang TY, Willmann JK. Acoustic and photoacoustic molecular imaging of cancer. J Nucl Med 2013; 54: 1851–1854. doi:10.2967/jnumed.112.115568.
16. Mahmood U, Weissleder R. Near-infrared optical imaging of proteases in cancer. Mol Cancer Ther 2003; 2: 489–496.
17. Elias DR, Thorek DLJ, Chen AK, Czupryna J, Tsourkas A. *In vivo* imaging of cancer biomarkers using activatable molecular probes. Cancer Biomark 2008; 4: 287–305.
18. Law B, Tung CH. Proteolysis: A biological process adapted in drug delivery, therapy, and imaging. Bioconjug Chem 2009; 20: 1683–1695. doi:10.1021/bc800500a.
19. Neefjes J, Dantuma NP. Fluorescent probes for proteolysis: Tools for drug discovery. Nat Rev Drug Discov 2004; 3: 58–69. doi:10.1038/nrd1282.
20. Chen X, Pradhan T, Wang F, Kim JS, Yoon J. Fluorescent chemosensors based on spiroring-opening of xanthenes and related derivatives. Chem Rev 2012; 112: 1910–1956. doi:10.1021/cr200201z.
21. McGrath WJ, Abola AP, Toledo D, Brown MT, Mangel WF. Characterization of human adenovirus proteinase activity in disrupted virus particles. Virology 1996; 217: 131–138. doi:10.1006/viro.1996.0100.
22. Van Noorden CJF, Boonacker E, Bissell ER, Meijer AJ, van Marle J, Smith RE. Ala-Pro-cresyl violet, a synthetic fluorogenic substrate for the analysis of kinetic parameters of dipeptidyl peptidase IV (CD26) in individual living rat hepatocytes. Anal Biochem 1997; 252: 71–77. doi:10.1006/abio.1997.2312.
23. Ho NH, Weissleder R, Tung CH. Development of a dual fluorogenic and chromogenic dipeptidyl peptidase IV substrate. Bioorg Med Chem Lett 2006; 16: 2599–2602. doi:10.1016/j.bmcl.2006.02.045.
24. Nicholls SB, Chu J, Abbruzzese G, Tremblay KD, Hardy JA. Mechanism of a genetically-encoded dark-to-bright reporter for caspase activity. J Biol Chem 2011; 286: 24977–24986. doi:10.1074/jbc.M111.221648.
25. Cai SX, Zhang HZ, Guastella J, Drewe J, Yang W, Weber E. Design and synthesis of rhodamine 110 derivative and caspase-3 substrate for enzyme- and cell-based fluorescent assay. Bioorg Med Chem Lett 2001; 11: 39–42. doi:10.1016/S0960-894X(00)00590-4.
26. Mitsunaga M, Kosaka N, Choyke PL, Young MR, Dextras CR, Saud SM, Colbrun NH, Sakabe M, Nagano T, Asanuma D, Urano Y, Kobayashi H. Fluorescence endoscopic detection of murine colitis-associated colon cancer by topically applied enzymatically rapid-activatable probe. Gut 2013; 62: 1179–1186. doi:10.1136/gutjnl-2011-301795.
27. Hettiarachchi SU, Prasai B, McCarley RL. Detection and cellular imaging of human cancer enzyme using a turn-on, wavelength-shiftable, self-immolative profluorophore. J Am Chem Soc 2014; 136: 7575–7578. doi:10.1021/ja5030707.
28. Weissleder R, Ntziachristos V. Shedding light onto live molecular targets. Nat Med 2003; 9: 123–128. doi:10.1038/nm0103-123.
29. Mahmood U, Tung CH, Bogdanov A Jr, Weissleder R. Near-infrared optical imaging of protease activity for tumor detection. Radiology 1999; 213: 866–870.
30. Lakowicz JR. Principles of Fluorescence Spectroscopy (Second edn). Kluwer Academic/Plenum Publishers: New York, 1999.
31. Weissleder R, Tung CH, Mahmood U, Bogdanov A Jr. *In vivo* imaging of tumors with protease-activated near-infrared fluorescent probes. Nat Biotechnol 1999; 17: 375–378. doi:10.1038/7933.
32. Ntziachristos V, Bremer C, Tung CH, Weissleder R. Imaging cathepsin B up-regulation in HT-1080 tumor models using fluorescence-mediated molecular tomography (FMT). Acad Radiol 2002; 9: S323–S325.
33. Chen J, Tung CH, Mahmood U, Ntziachristos V, Gyurko R, Fishman MC, Huang PL, Weissleder R. *In vivo* imaging of proteolytic activity in atherosclerosis. Circulation 2002; 105: 2766–2771. doi:10.1161/01.CIR.0000017860.20619.23.
34. Wunder A, Tung CH, Müller-Ladner U, Weissleder R, Mahmood U. *In vivo* imaging of protease activity in arthritis: A novel approach for monitoring treatment response. Arthritis Rheum 2004; 50: 2459–2465. doi:10.1002/art.20379.
35. Jaffer FA, Vinegoni C, John MC, Aikawa E, Gold HK, Finn AV, Ntziachristos V, Libby P, Weissleder R. Real-time catheter molecular sensing of inflammation in proteolytically active

atherosclerosis. Circulation 2008; 118: 1802–1809. doi:10.1161/CIRCULATIONAHA.108.785881.
36. Messerli SM, Prabhakar S, Tang Y, Shah K, Cortes ML, Murthy V, Weissleder R, Breakfield XO, Tung CH. A novel method for imaging apoptosis using a caspase-1 near-infrared fluorescent probe. Neoplasia 2004; 6: 95–105.
37. Tung CH, Mahmood U, Bredow S, Weissleder R. *In vivo* imaging of proteolytic enzyme activity using a novel molecular reporter. Cancer Res 2000; 60: 4953–4958.
38. Abd-Elgaliel WR, Cruz-Monserrate Z, Logsdon C, Tung CH. Molecular imaging of cathepsin E-positive tumors in mice using a novel protease-activatable fluorescent probe. Mol Biosyst 2011; 7: 3207–3213. doi:10.1039/C1MB05215B.
39. Jaffer FA, Kim DE, Quinti L, Tung CH, Aikawa E, Pande AN, Kohler RH, Shi GP, Libby P, Weissleder R. Optical visualization of cathepsin K activity in atherosclerosis with a novel protease-activatable fluorescence sensor. Circulation 2007; 115: 2292–2298. doi:10.1161/CIRCULATIONAHA.106.660340.
40. Shah K, Tung CH, Chang CH, Slootweg E, O'Loughlin T, Breakefield XO, Weissleder R. *In vivo* imaging of HIV protease activity in amplicon vector-transduced gliomas. Cancer Res 2004; 64: 273–278. doi:10.1158/0008-5472.CAN-03-1123.
41. Law B, Curino A, Bugge TH, Weissleder R, Tung CH. Design, synthesis, and characterization of urokinase plasminogen-activator sensitive near-infrared reporter. Chem Biol 2004; 11: 99–106. doi:10.1016/j.chembiol.2003.12.017.
42. Bremer C, Tung CH, Bogdanov A, Weissleder R. Imaging of differential protease expression in breast cancers for detection of aggressive tumor phenotypes. Radiology 2002; 222: 814–818. doi:10.1148/radiol.2223010812.
43. Bremer C, Bredow S, Mahmood U, Weissleder R, Tung CH. Optical imaging of matrix metalloproteinase-2 activity in tumors: Feasibility study in a mouse model. Radiology 2001; 221: 523–529. doi:10.1148/radiol.2212010368.
44. Bremer C, Tung CH, Weissleder R. *In vivo* molecular target assessment of matrix metalloproteinase inhibition. Nat Med 2001; 7: 743–748. doi:10.1038/89126.
45. Bremer C, Tung CH, Weissleder R. Molecular imaging of MMP expression and therapeutic MMP inhibition. Acad Radiol 2002; 9: S314–315.
46. Chen J, Tung CH, Allport JR, Chen S, Weissleder R, Huang PL. Near-infrared fluorescent imaging of matrix metalloproteinase activity after myocardial infarction. Circulation 2005; 111: 1800–1805. doi:10.1161/01.CIR.0000160936.91849.9F.
47. Deguchi JO, Aikawa M, Tung CH, Aikawa E, Kim DE, Ntziachristos V, Weissleder R, Libby P. Inflammation in atherosclerosis: Visualizing matrix metalloproteinase action in macrophages *in vivo*. Circulation 2006; 114: 55–62. doi:10.1161/CIRCULATIONAHA.106.619056.
48. Von Burstin J, Eser S, Seidler B, Meining A, Bajbouj M, Mages J, Lang R, Kind AJ, Schnieke AE, Schmid RM, Schneider G, Saur D. Highly sensitive detection of early-stage pancreatic cancer by multimodal near-infrared molecular imaging in living mice. Int J Cancer 2008; 123: 2138–2147. doi:10.1002/ijc.23780.
49. Sheth RA, Kunin A, Stangenberg L, Sinnamon M, Hung KE, Kucherlapati R, Mahmood U. *In vivo* optical molecular imaging of matrix metalloproteinase activity following celecoxib therapy for colorectal cancer. Mol Imaging 2012; 11: 417–425.
50. Onda N, Kemmochi S, Morita R, Ishihara Y, Shibutani M. *In vivo* imaging of tissue-remodeling activity involving infiltration of macrophages by a systemically administered protease-activatable probe in colon cancer tissues. Transl Oncol 2013; 6: 628–637.
51. Cuneo KC, Mito JK, Javid MP, Ferrer JM, Kim Y, Lee WD, Bawendi MG, Brigman BE, Kirsch DG. Imaging primary mouse sarcomas after radiation therapy using cathepsin-activatable fluorescent imaging agents. Int J Radiat Oncol Biol Phys 2013; 86: 136–142. doi:10.1016/j.ijrobp.2012.12.007.
52. Ding S, Eric Blue R, Chen Y, Scull B, Kay Lund P, Morgan D. Molecular imaging of gastric neoplasia with near-infrared fluorescent activatable probes. Mol Imaging 2012; 11: 507–515.
53. Zhang J, Preda DV, Vasquez KO, Morin J, Delaney J, Bao B, Percival MD, Xu D, McKay D, Klimas M, Bednar B, Sur C, Gao DZ, Madden K, Yared W, Rajopadhye M, Peterson JD. A fluorogenic near-infrared imaging agent for quantifying plasma and local tissue renin activity *in vivo* and *ex vivo*. Am J Physiol Renal Physiol 2012; 303: F593–F603. doi:10.1152/ajprenal.00361.2011.
54. Barber PA, Rushforth D, Agrawal S, Tuor UI. Infrared optical imaging of matrix metalloproteinases (MMPs) up regulation following ischemia reperfusion is ameliorated by hypothermia. BMC Neurosci 2012; 13: 76. doi:10.1186/1471-2202-13–76.
55. Al Rawashdeh W, Arns S, Gremse F, Ehling J, Knüchel-Clarke R, Kray S, Spöler F, Kiessling F, Lederle W. Optical tomography of MMP activity allows a sensitive noninvasive characterization of the invasiveness and angiogenesis of SCC xenografts. Neoplasia 2014; 16: 235–246. doi:10.1016/j.neo.2014.03.005.
56. Waschkau B, Faust A, Schäfers M, Bremer C. Performance of a new fluorescence-labeled MMP inhibitor to image tumor MMP activity *in vivo* in comparison to an MMP-activatable probe. Contrast Media Mol Imaging 2013; 8: 1–11. doi:10.1002/cmmi.1486.
57. Hollis CP, Weiss HL, Evers BM, Gemeinhart RA, Li T. *In vivo* investigation of hybrid paclitaxel nanocrystals with dual fluorescent probes for cancer theranostics. Pharm Res 2013. doi:10.1007/s11095-013-1048-x.
58. Eaton VL, Vasquez KO, Goings GE, Hunter ZN, Peterson JD, Miller SD. Optical tomographic imaging of near infrared imaging agents quantifies disease severity and immunomodulation of experimental autoimmune encephalomyelitis *in vivo*. J Neuroinflammation 2013; 10: 138. doi:10.1186/1742-2094-10-138.
59. Mitra S, Modi KD, Foster TH. Enzyme-activatable imaging probe reveals enhanced neutrophil elastase activity in tumors following photodynamic therapy. J Biomed Opt 2013; 18: 101314. doi:10.1117/1.JBO.18.10.101314.
60. Sarkar N, Banerjee J, Hanson AJ, Elegbede AI, Rosendahl T, Krueger AB, Banerjee AL, Tobwala S, Wang R, Lu X, Mallik S, Srivastava DK. Matrix metalloproteinase-assisted triggered release of liposomal contents. Bioconjug Chem 2008; 19: 57–64. doi:10.1021/bc070081p.
61. Elegbede AI, Banerjee J, Hanson AJ, Tobwala S, Ganguli B, Wang R, Lu X, Srivastava DK, Mallik S. Mechanistic studies on the triggered release of liposomal contents by matrix metalloproteinase-9. J Am Chem Soc 2008; 130: 10633–10642. doi:10.1021/ja801548g.
62. Malik R, Qian S, Law B. Design and synthesis of a near-infrared fluorescent nanofiber precursor for detecting cell-secreted urokinase activity. Anal Biochem 2011; 412: 26–33. doi:10.1016/j.ab.2011.01.010.
63. Akers WJ, Xu B, Lee H, Sudlow GP, Fields GB, Achilefu S, Edwards WB. Detection of MMP-2 and MMP-9 activity *in vivo* with a triple-helical peptide optical probe. Bioconjug Chem 2012; 23: 656–663. doi:10.1021/bc300027y.
64. Mok H, Jeong H, Kim SJ, Chung BH. Indocyanine green encapsulated nanogels for hyaluronidase activatable and selective near infrared imaging of tumors and lymph nodes. Chem Commun 2012; 48: 8628–8630. doi:10.1039/c2cc33555g.
65. Mahajan NP, Harrison-Shostak DC, Michaux J, Herman B. Novel mutant green fluorescent protein protease substrates reveal the activation of specific caspases during apoptosis. Chem Biol 1999; 6: 401–409. doi:10.1016/S1074-5521(99)80051-9.
66. Zhang J, Ma Y, Taylor SS, Tsien RY. Genetically encoded reporters of protein kinase A activity reveal impact of substrate tethering. Proc Natl Acad Sci U S A 2001; 98: 14997–15002. doi:10.1073/pnas.211566798.
67. Yang J, Zhang Z, Lin J, Lu J, Biu BF, Zeng S, Luo Q. Detection of MMP activity in living cells by a genetically encoded surface-displayed FRET sensor. Biochim Biophys Acta 2007; 1773: 400–407. doi:10.1016/j.bbamcr.2006.11.002.
68. Zhang Z, Yang J, Lu J, Lin J, Zeng S, Luo Q. Fluorescence imaging to assess the matrix metalloproteinase activity and its inhibitor *in vivo*. J Biomed Opt 2008; 13: 011006. doi:10.1117/1.2830659.
69. Ouyang M, Huang H, Shaner NC, Remacle AG, Shiryaev SA, Strongin AY, Tsien RY, Wang Y. Simultaneous visualization of protumorigenic Src and MT1-MMP activities with fluorescence resonance energy transfer. Cancer Res 2010; 70: 2204–2212. doi:10.1158/0008-5472.CAN-09-3698.
70. Pham W, Choi Y, Weissleder R, Tung CH. Developing a peptide-based near-infrared molecular probe for protease sensing. Bioconjug Chem 2004; 15: 1403–1407. doi:10.1021/bc049924s.
71. McIntyre JO, Fingleton B, Wells KS, Piston DW, Lynch CC, Gautam S, Matrisian LM. Development of a novel fluorogenic proteolytic beacon for *in vivo* detection and imaging of tumour-associated matrix metalloproteinase-7 activity. Biochem J 2004; 377: 617–628. doi:10.1042/BJ20030582.

72. Lee S, Park K, Lee SY, Ryu JH, Park JW, Ahn HJ, Kwon IC, Youn IC, Kim K, Choi K. Dark quenched matrix metalloproteinase fluorogenic probe for imaging osteoarthritis development *in vivo*. Bioconjug Chem 2008; 19: 1743–1747. doi:10.1021/bc800264z.
73. Yoon SM, Myung SJ, Kim IW, Do EJ, Ye BD, Ryu JH, Park K, Kim K, Kwon IC, Kim MJ, Moon DH, Yang DH, Kim KJ, Byeon JS, Yang SK, Kim JH. Application of near-infrared fluorescence imaging using a polymeric nanoparticle-based probe for the diagnosis and therapeutic monitoring of colon cancer. Dig Dis Sci 2011; 56: 3005–3013. doi:10.1007/s10620-011-1685-z.
74. Lin X, Xie J, Zhu L, Lee S, Niu G, Ma Y, Kim K, Chen X. Hybrid ferritin nanoparticles as activatable probes for tumor targeting. Angew Chem Int Ed Engl 2011; 50: 1569–1572. doi:10.1002/anie.201006757.
75. Liu TW, Akens MK, Chen J, Wise-Milestone L, Wilson BC, Zheng G. Imaging of specific activation of photodynamic molecular beacons in breast cancer vertebral metastases. Bioconjug Chem 2011; 22: 1021–1030. doi:10.1021/bc200169x.
76. Moss ML, Rasmussen FH. Fluorescent substrates for the proteinases ADAM17, ADAM10, ADAM8, and ADAM12 useful for high-throughput inhibitor screening. Anal Biochem 2007; 366: 144–148. doi:10.1016/j.ab.2007.04.043.
77. Zhu L, Xie J, Swierczewska M, Zhang F, Lin X, Fang X, Niu G, Lee S, Chen X. Dual-functional, receptor-targeted fluorogenic probe for *in vivo* imaging of extracellular protease expressions. Bioconjug Chem 2011; 22: 1001–1005. doi:10.1021/bc200005w.
78. Zhu L, Xie J, Swierczewska M, Zhang F, Quan Q, Ma Y, Fang X, Kim K, Lee S, Chen X. Real-time video imaging of protease expression *in vivo*. Theranostics 2011; 1: 18–27. doi:10.7150/thno/v01p0018.
79. Zhu L, Zhang F, Ma Y, Liu G, Kim K, Fang X, Lee S, Chen X. *In vivo* optical imaging of membrane-type matrix metalloproteinase (MT-MMP) activity. Mol Pharmaceutics 2011; 8: 2331–2338. doi:10.1021/mp2002297.
80. Zhu L, Ma Y, Kiesewetter DO, Wang Y, Lang L, Lee S, Niu G, Chen X. Rational design of matrix metalloproteinase-13 activatable probes for enhanced specificity. ACS Chem Biol 2014; 9: 510–516. doi:10.1021/cb400698s.
81. Li J, Chen K, Liu H, Cheng K, Yang M, Zhang J, Cheng JD, Zhang Y, Cheng Z. Activatable near-infrared fluorescent probe for *in vivo* imaging of fibroblast activation protein-alpha. Bioconjug Chem 2012; 23: 1704–1711. doi:10.1021/bc300278r.
82. Huang CW, Li Z, Conti PS. Radioactive smart probe for potential corrected matrix metalloproteinase imaging. Bioconjug Chem 2012; 23: 2159–2167. doi:10.1021/bc3001968.
83. Lim NH, Meinjohanns E, Bou-Gharios G, Gompels LL, Nuti E, Rossello A, Devel L, Dive V, Meldal M, Nagase H. *In vivo* imaging of matrix metalloproteinase 12 and matrix metalloproteinase 13 activities in the mouse model of collagen-induced arthritis. Arthritis Rheumatol 2014; 66: 589–598. doi:10.1002/art.38295.
84. Bullok K, Piwnica-Worms D. Synthesis and characterization of a small, membrane-permeant, caspase-activatable far-red fluorescent peptide for imaging apoptosis. J Med Chem 2005; 48: 5404–5407. doi:10.1021/jm050008p.
85. Bullok KE, Maxwell D, Kesarwala AH, Gammon S, Prior JL, Snow M, Stanley S, Piwnica-Worms D. Biochemical and *in vivo* characterization of a small, membrane-permeant, caspase-activatable far-red fluorescent peptide for imaging apoptosis. Biochemistry 2007; 46: 4055–4065. doi:10.1021/bi061959n.
86. Maxwell D, Chang Q, Zhang X, Barnett EM, Piwnica-Worms D. An improved cell-penetrating, caspase-activatable, near-infrared fluorescent peptide for apoptosis imaging. Bioconjug Chem 2009; 20: 702–709. doi:10.1021/bc800516n.
87. Johnson JR, Kocher B, Barnett EM, Marasa J, Piwnica-Worms D. Caspase-activated cell-penetrating peptides reveal temporal coupling between endosomal release and apoptosis in an RGC-5 cell model. Bioconjug Chem 2012; 23: 1783–1793l. doi:10.1021/bc300036z.
88. Qiu X, Johnson JR, Wilson BS, Gammon ST, Piwnica-Worms D, Barnett EM. Single-cell resolution imaging of retinal ganglion cell apoptosis *in vivo* using a cell-penetrating caspase-activatable peptide probe. PLoS One 2014; 9: e88855; doi: 10.1371/journal.pone.0088855.
89. Gong P, Shi B, Zhang P, Hu D, Zheng M, Zheng C, Gao D, Cai L. DNase-activatable fluorescence probes visualizing the degradation of exogenous DNA in living cells. Nanoscale 2012; 4: 2454–2462. doi:10.1039/c2nr12005d.
90. Edgington LE, Bogyo M. *In vivo* imaging and biochemical characterization of protease function using fluorescent activity-based probes. Curr Protoc Chem Biol 2013; 5: 25–44. doi:10.1002/9780470559277.ch120235.
91. Blum G, Mullins SR, Keren K, Fonovic M, Jedeszko C, Rice MJ, Sloane BF, Bogyo M. Dynamic imaging of protease activity with fluorescently quenched activity-based probes. Nat Chem Biol 2005; 1: 203–209. doi:10.1038/nchembio728.
92. Verdoes M, Edgington LE, Scheeren FA, Leyva M, Blum G, Weiskopf K, Bachmann MH, Ellman JA, Bogyo M. A nonpeptidic cathpesin S activity-based probe for noninvasive optical imaging of tumor-associated macrophages. Chem Biol 2012; 19: 619–628. doi:10.1016/j.chembiol.2012.03.012.
93. Lee S, Cha EJ, Park K, Lee SY, Hong JK, Sun IC, Kim SY, Choi K, Kwon IC, Kim K, Ahn CH. A near-infrared-fluorescence-quenched gold-nanoparticle imaging probe for *in vivo* drug screening and protease activity determination. Angew Chem Int Ed Engl 2008; 120: 2846–2849. doi:10.1002/anie.200705240.
94. Kim YP, Oh YH, Oh E, Ko S, Han MK, Kim HS. Energy transfer-based multiplexed assay of proteases by using gold nanoparticle and quantum dot conjugates on a surface. Anal Chem 2008; 80: 4634–4641. doi:10.1021/ac702416e.
95. Chang E, Miller JS, Sun J, Yu WW, Colvin VL, Drezek R, West JL. Protease-activated quantum dot probes. Biochem Biophys Res Commun 2005; 334: 1317–1321. doi:10.1016/j.bbrc.2005.07.028.
96. Shcherbakova DM, Verkhusha VV. Near-infrared fluorescent proteins for multicolor in *vivo* imaging. Nat Methods 2013; 10: 751–754. doi:10.1038/nmeth.2521.
97. Jiguet-Jiglaire C, Cayol M, Mathieu S, Jeanneau C, Bouvier-Labit C, Ouafik L, El-Battari A. Noninvasive near-infared fluorescent protein-based imaging of tumor progression and metastases in deep organs and intraosseous tissues. J Biomed Opt 2014; 19: 16019. doi:10.1117/1.JBO.19.1.016019.
98. Michalet X, Pinaud FF, Bentolila LA, Tsay JM, Doose S, Li JJ, Sundaresan G, Wu AM, Gambhir SS, Weiss S. Quantum dots for live cells, *in vivo* imaging, and diagnostics. Science 2005; 307: 538–544. doi:10.1126/science.1104274.
99. Kersemans V, Cornelissen B. Targeting the tumour: Cell penetrating peptides for molecular imaging and radiotherapy. Pharmaceuticals 2010; 3: 600–620. doi:10.3390/ph3030600.
100. Phillips E, Penate-Medina O, Zanzonico PB, Carvajal RD, Mohan P, Ye Y, Humm J, Gönen M, Kalaigian H, Schöder H, Strauss HW, Larson SM, Wiesner U, Bradbury MS. Clinical translation of an ultrasmall inorganic-PET imaging nanoparticle probe. Sci Transl Med 2014; 6: 260ra149; doi: 10.1126/scitranslmed.3009524
101. Choi HS, Liu W, Misra P, Tanaka E, Zimmer JP, Ipe BI, Bawendi MG, Frangioni JV. Renal clearance of nanoparticles. Nat Biotechnol 2007; 25: 1165–1170. doi:10.1038/nbt1340.
102. Lovell JF, Liu TWB, Chen J, Zheng G. Activatable photosensitizers for imaging and therapy. Chem Rev 2010; 110: 2839–2857. doi:10.1021/cr900236h.
103. Chen J, Stefflova K, Niedre MJ, Wilson BC, Chance B, Glickson JD, Zheng G. Protease-triggered photosensitizing beacon based on singlet oxygen quenching and activation. J Am Chem Soc 2004; 126: 11450–11451. doi:10.1021/ja047392k.
104. Stefflova K, Chen J, Li H, Zheng G. Targeted photodynamic therapy agent with a built-in apoptosis sensor for *in vivo* near-infrared imaging of tumor apoptosis triggered by its photosensitization *in situ*. Mol Imaging 2006; 5: 520–532.
105. Zheng G, Chen J, Stefflova K, Jarvi M, Li H, Wilson BC. Photodynamic molecular beacon as an activatable photosensitizer based on protease-controlled singlet oxygen quenching and activation. Proc Natl Acad Sci U S A 2007; 104: 8989–8994. doi:10.1073/pnas.0611142104.
106. Lo P, Chen J, Stefflova K, Warren MS, Navab R, Bandarchi B, Mullins S, Tsao M, Cheng JD, Zheng G. Photodynamic molecular beacon triggered by fibroblast activation protein on cancer-associated fibroblasts for diagnosis and treatment of epithelial cancers. J Med Chem 2009; 52: 358–368. doi:10.1021/jm801052f.
107. Agostinis P, Berg K, Cengel KA, Foster TH, Girotti AW, Gollnick SO, Hahn SM, Hamblin MR, Juzeniene A, Kessel D, Korbelik M, Moan J, Mroz P, Nowis D, Piette J, Wilson BC, Golab J. Photodynamic

therapy of cancer: An update. CA Cancer J Clin 2011; 61: 250–281. doi:10.3322/caac.20114.
108. Marques SM, Esteves da Silva JC. Firefly bioluminescence: A mechanistic approach of luciferase catalyzed reactions. IUBMB Life 2009; 61: 6–17. doi:10.1002/iub.134.
109. Wehrman TS, von Degenfeld G, Krutzik PO, Nolan GP, Blau HM. Luminescent imaging of beta-galactosidase activity in living subjects using sequential reporter-enzyme luminescence. Nat Methods 2006; 3: 295–301. doi:10.1038/nmeth868.
110. Yao H, So MK, Rao J. A bioluminogenic substrate for *in vivo* imaging of ß-lactamase activity. Angew Chem Int Ed Engl 2007; 46: 7031–7034. doi:10.1002/anie.200701931.
111. Shah K, Tung CH, Breakefield XO, Weissleder R. *In vivo* imaging of S-TRAIL-mediated tumor regression and apoptosis. Mol Ther 2005; 11: 926–931. doi:10.1016/j.ymthe.2005.01.017.
112. Dragulescu-Andrasi A, Liang G, Rao J. *In vivo* bioluminescence imaging of furin activity in breast cancer cells using bioluminogenic substrates. Bioconjug Chem 2009; 20: 1660–1666. doi:10.1021/bc9002508.
113. Godinat A, Park HM, Miller SC, Cheng K, Hanahan D, Sanman LE, Bogyo M, Yu A, Nikitin GF, Stahl A, Dubikovskaya EA. A biocompatible *in vivo* ligation reaction and its application for non-invasive bioluminescent imaging or protease activity in living mice. ACS Chem Biol 2013; 8: 987–999. doi:10.1021/cb3007314.
114. Mofford DM, Reddy GR, Miller SC. Latent luciferase activity in the fruit fly revealed by a synthetic luciferin. Proc Natl Acad Sci U S A 2014; 111: 4443–4448. doi:10.1073/pnas.1319300111.
115. Kneen M, Farinas J, Li Y, Verkman AS. Green fluorescent protein as a noninvasive intracellular pH indicator. Biophys J 1998; 74: 1591–1599. doi:10.1016/S0006-3495(98)77870-1.
116. Han J, Burgess K. Fluorescent indicators for intracellular pH. Chem Rev 2010; 110: 2709–2728. doi:10.1021/cr900249z.
117. Hilderbrand SA, Kelly KA, Niedre M, Weissleder R. Near infrared fluorescence-based bacteriophage particles for ratiometric pH imaging. Bioconjug Chem 2008; 19: 1635–1639. doi:10.1021/bc800188p.
118. Hilderbrand SA, Weissleder R. Optimized pH responsive cyanine fluorochromes for detection of acidic environments. Chem Commun 2007: 2747–2749. doi:10.1039/B703764C.
119. Kirpotin D, Hong K, Mullah N, Papahadjopoulos D, Zalipsky S. Liposomes with detachable polymer coating: Destabilization and fusion of dioleoylphosphatidelyethanolamine vesicles triggered by cleavage of surface-grafted poly(ethylene glycol). FEBS Lett 1996; 388: 115–118. doi:10.1016/0014-5793(96)00521-2.
120. Bellomo EG, Wyrsta MD, Pakstis L, Pochan DJ, Deming TJ. Stimuli-responsive polypeptide vesicles by conformation-specific assembly. Nature Mat 2004; 3: 244–248. doi:10.1038/nmat1093.
121. Park HS, Lee JE, Cho MY, Noh YW, Sung MH, Poo H, Hong KS, Lim YT. pH-stimuli-responsive near-infrared optical imaging nanoprobe based on poly(γ-glutamic acid)/poly(β-amino ester) nanoparticles. Nanotechnology 2011; 22: 465603. doi:10.1088/0957-4484/22/46/465603.
122. Urano Y, Asanuma D, Hama Y, Koyama Y, Barrett T, Kamiya M, Nagano T, Watanabe T, Hasegawa A, Choyke PL, Kobayashi H. Selective molecular imaging of viable cancer cells with pH-activatable fluorescence probes. Nat Med 2009; 15: 104–109. doi:10.1038/nm.1854.
123. Ogawa M, Kosaka N, Regino CA, Mitsunaga M, Choyke PL, Kobayashi H. High sensitivity detection of cancer *in vivo* using a dual-controlled activation fluorescent imaging probe based on H-dimer formation and pH activation. Mol Biosyst 2010; 6: 888–893. doi:10.1039/b917876g.
124. Lee H, Akers W, Bhushan K, Bloch S, Sudlow G, Tang R, Achilefu S. Near-infrared pH-activatable fluorescent probes for imaging primary and metastatic breast tumors. Bioconjug Chem 2011; 22: 777–784. doi:10.1021/bc100584d.
125. Sethuraman VA, Bae YH. TAT peptide-based micelle system for potential active targeting of anti-cancer agents to acidic solid tumors. J Control Release 2007; 118: 216–224. doi:10.1016/j.conrel.2006.12.008.
126. Wang Z, Zhang X, Huang P, Zhao W, Liu D, Nie L, Yue X, Wang S, Ma Y, Kiesewetter D, Niu G, Chen X. Dual-factor triggered fluorogenic nanoprobe for ultrahigh contrast and subdiffraction fluorescence imaging. Biomaterials 2013; 34: 6194–6201. doi:10.1016/j.biomaterials.2013.05.004.
127. Liu XD, Xu Y, Sun R, Xu YJ, Lu JM, Ge JF. A coumarin-indole-based near-infrared ratiometric pH probe for intracellular fluorescence imaging. Analyst 2013; 138: 6542–6550. doi:10.1039/c3an01033c.
128. Wang L, Zhu X, Xie C, Ding N, Weng X, Lu W, Wei X, Li C. Imaging acidosis in tumors using a pH-activated near-infrared fluorescence probe. Chem Commun 2012; 48: 11677–11679. doi:10.1039/c2cc36488c.
129. Zhao Y, Ji T, Wang H, Li S, Zhao Y, Nie G. Self-assembled peptide nanoparticles as tumor microenvironment activatable probes for tumor targeting and imaging. J Control Release 2014; 177: 11–19. doi:10.1016/j.jconrel.2013.12.037.
130. Danhier F, Feron O, Préat V. To exploit the tumor microenvironment: Passive and active tumor targeting of nanocarriers for anticancer drug delivery. J Control Release 2010; 148: 135–146.
131. Finkel T, Serrano M, Blasco MA. The common biology of cancer and ageing. Nature 2007; 448: 767–774. doi:10.1038/nature05985.
132. Zweier JL, Hassan Talukder MA. The role of oxidants and free radicals in reperfusion injury. Cardiovasc Res 2006; 70: 181–190. doi:10.1016/j.cardiores.2006.02.025.
133. Kobayashi H, Ogawa M, Alford R, Choyke PL, Urano Y. New strategies for fluorescent probe design in medical diagnostic imaging. Chem Rev 2010; 110: 2620–2640. doi:10.1021/cr900263j.
134. Chang MCY, Pralle A, Isacoff EY, Chang CJ. A selective, cell-permeable optical probe for hydrogen peroxide in living cells. J Am Chem Soc 2004; 126: 15392–15393. doi:10.1021/ja0441716.
135. Miller EW, Albers AE, Pralle A, Isacoff EY, Chang CJ. Boronate-based fluorescent probes for imaging cellular hydrogen peroxide. J Am Chem Soc 2005; 127: 16652–16659. doi:10.1021/ja054474f.
136. Miller EW, Tulyathan O, Isacoff EY, Chang CJ. Molecular imaging of hydrogen peroxide produced for cell signaling. Nat Chem Biol 2007; 3: 263–267. doi:10.1038/nchembio871.
137. Dickinson BC, Chang CJ. A targetable fluorescent probe for imaging hydrogen peroxide in the mitochondria of living cells. J Am Chem Soc 2008; 130: 11561. doi:10.1021/ja802355u.
138. Abo M, Urano Y, Hanaoka K, Terai T, Komatsu T, Nagano T. Development of a highly sensitive fluorescence probe for hydrogen peroxide. J Am Chem Soc 2011; 133: 10629–10637. doi:10.1021/ja203521e.
139. Dickinson BC, Huynh C, Chang CJ. A palette of fluorescent probes with varying emission colors for imaging hydrogen peroxide signaling in living cells. J Am Chem Soc 2010; 132: 5906–5915. doi:10.1021/ja1014103.
140. Ye Z, Chen J, Wang G, Yuan J. Development of a terbium complex-based luminescent probe for imaging endogenous hydrogen peroxide generation in plant tissues. Anal Chem 2011; 83: 4163–4169. doi:10.1021/ac200438g.
141. Kim G, Koo Lee YE, Xu H, Philbert MA, Kopelman R. Nanoencapsulation method for high selectivity sensing of hydrogen peroxide inside live cells. Anal Chem 2010; 82: 2165–2169. doi:10.1021/ac9024544.
142. Panizzi P, Nahrendorf M, Wildgruber M, Waterman P, Figueiredo JL, Aikawa E, McCarthy J, Weissleder R, Hilderbrand SA. Oxazine conjugated nanoparticle detects *in vivo* hypochlorous acid and peroxynitrite generation. J Am Chem Soc 2009; 131: 15739–15744. doi:10.1021/ja903922u.
143. Yang D, Sun ZN, Peng T, Wang HL, Shen JG, Chen Y, Tam PK. Synthetic fluorescent probe for imaging of peroxynitrite and hypochlorous acid in living cells. Methods Mol Biol 2010; 591: 93–103. doi:10.1007/978-1-60761-404-3_5.
144. Koide Y, Urano Y, Kenmoku S, Kojima H, Nagano T. Design and synthesis of fluorescent probes for selective detection of highly reactive oxygen species in mitochondria of living cells. J Am Chem Soc 2007; 129: 10324–10325. doi:10.1021/ja073220m.
145. Yang D, Wang HL, Sun ZN, Chung NW, Shen JG. A highly selective fluorescent probe for the detection and imaging of peroxynitrite in living cells. J Am Chem Soc 2006; 128: 6004–6005. doi:10.1021/ja0603756.
146. Sun ZN, Wang HL, Liu FQ, Chen Y, Tam PK, Yang D. BODIPY-based fluorescent probe for peroxynitrite detection and imaging in living cells. Org Lett 2009; 11: 1887–1890. doi:10.1021/ol900279z.
147. Maeda H, Yamamoto K, Nomura Y, Kohno I, Hafsi L, Ueda N, Yoshida S, Fukuda M, Fukuyasu Y, Yamauchi Y, Itoh N. A design of fluorescent probes for superoxide based on a nonredox mechanism. J Am Chem Soc 2005; 127: 68–69. doi:10.1021/ja047018k.

148. Xu K, Liu X, Tang B, Yang G, Yang Y, An L. Design of a phosphinate-based fluorescent probe for superoxide detection in mouse peritoneal macrophages. Chemistry 2007; 13: 1411–1416. doi:10.1002/chem.200600497.
149. Maeda H, Yamamoto K, Kohno I, Hafsi L, Itoh N, Nakagawa S, Kanagawa N, Suzuki K, Uno T. Design of a practical fluorescent probe for superoxide based protection-deprotection chemistry of fluoresceins with benzenesulfonyl protecting group. Chemistry 2007; 13: 1946–1954. doi:10.1002/chem.200600522.
150. Sasaki E, Kojima H, Nishimatsu H, Urano Y, Kikuchi K, Hirata Y, Nagano T. Highly sensitive near-infrared fluorescent probes for nitric oxide and their application to isolated organs. J Am Chem Soc 2005; 127: 3684–3685. doi:10.1021/ja042967z.
151. Lim MH, Xu D, Lippard SJ. Visualization of nitric oxide in living cells by a copper-based fluorescent probe. Nat Chem Biol 2006; 2: 375–380. doi:10.1038/nchembio794.
152. Pluth MD, McQuade LE, Lippard SJ. Cell-trappable fluorescent probes for nitric oxide visualization in living cells. Org Lett 2010; 12: 2318–2321. doi:10.1021/ol1006289.
153. Kenmoku S, Urano Y, Kojima H, Nagano T. Development of a highly specific rhodamine-based fluorescence probe for hypochlorous acid and its application to real-time imaging of phagocytosis. J Am Chem Soc 2007; 129: 7313–7318. doi:10.1021/ja068740g.
154. Sun ZN, Liu FQ, Chen Y, Tam PK, Yang D. A highly specific BODIPY-based fluorescent probe for the detection of hypochlorous acid. Org Lett 2008; 10: 2171–2174. doi:10.1021/ol800507m.
155. Yang YK, Cho HJ, Lee J, Shin I, Tae J. A rhodamine-hydroxamic acid-based fluorescent probe for hypochlorous acid and its applications to biological imagings. Org Lett 2009; 11: 859–861. doi:10.1021/ol802822t.
156. Manevich Y, Held KD, Biaglow JE. Coumarin-3-carboxylic acid as a detector for hydroxyl radicals generated chemically and by gamma radiation. Radiat Res 1997; 148: 580–591.
157. Ganea GM, Kolic PE, El-Zahab B, Warner IM. Ratiometric coumarin-neutral red (CONER) nanoprobe for detection of hydroxyl radicals. Anal Chem 2011; 83: 2576–2581. doi:10.1021/ac102874x.
158. Albers AE, Okreglak VS, Chang CJ. A FRET-based approach to ratiometric fluorescence detection of hydrogen peroxide. J Am Chem Soc 2006; 128: 9640–9641. doi:10.1021/ja063308k.
159. Srikun D, Miller EW, Domaille DW, Chang CJ. An ICT-based approach to ratiometric fluorescence imaging of hydrogen peroxide produced in living cells. J Am Chem Soc 2008; 130: 4596–4597. doi:10.1021/ja711480f.
160. Li C, Hu J, Liu T, Liu S. Stimuli-triggered off/on switchable complexation between a novel type of charge-generation polymer (CGP) and gold nanoparticles for the sensitive colorimetric detection of hydrogen peroxide and glucose. Macromolecules 2011; 44: 429–431. doi:10.1021/ma102608a.
161. Belousov VV, Fradkov AF, Lukyanov KA, Staroverov DB, Shakhbazov KS, Terskikh AV, Lukyanov S. Genetically encoded fluorescent indicator for intracellular hydrogen peroxide. Nat Methods 2006; 3: 281–286. doi:10.1038/nmeth866.
162. Wang W, Fang H, Groom L, Cheng A, Zhang W, Liu J, Wang X, Li K, Han P, Zheng M, Yin J, Wang W, Mattson MP, Kao JP, Lakatta EG, Sheu SS, Ouyang K, Chen J, Dirksen RT, Cheng H. Superoxide flashes in single mitochondria. Cell 2008; 134: 279–290. doi:10.1016/j.cell.2008.06.017.
163. Zhao BS, Liang Y, Song Y, Zheng C, Hao Z, Chen PR. A highly selective fluorescent probe for visualization of organic hydroperoxides in living cells. J Am Chem Soc 2010; 132: 17065–17067. doi:10.1021/ja1071114.
164. Lee D, Khaja S, Velasquez-Castano JC, Dasari M, Sun C, Petros J, Taylor WR, Murthy N. *In vivo* imaging of hydrogen peroxide with chemiluminescent nanoparticles. Nat Mater 2007; 6: 765–769. doi:10.1038/nmat1983.
165. Van de Bittner GC, Dubikovskaya EA, Bertozzi CR, Chang CJ. *In vivo* imaging of hydrogen peroxide production in a murine tumor model with a chemoselective bioluminescent reporter. Proc Natl Acad Sci U S A 2010; 107: 21316–21321. doi:10.1073/pnas.1012864107.
166. Van de Bittner GC, Bertozzi CR, Chang CJ. A strategy for dual-analyte luciferin imaging: *In vivo* bioluminescence detection of hydrogen peroxide and caspase activity in a murine model of acute inflammation. J Am Chem Soc 2013; 135: 1783–1795. doi:10.1021/ja309078t.
167. Weinstain R, Savariar EN, Felsen CN, Tsien RY. *In vivo* targeting of hydrogen peroxide by activatable cell-penetrating peptides. J Am Chem Soc 2014; 136: 874–877. doi:10.1021/ja411547j.
168. Imamura H, Huynh Nhat KP, Togawa H, Saito K, Iino R, Kato-Yamada Y, Nagai T, Noji H. Visualization of ATP levels inside single living cells with fluorescence resonance energy transfer-based genetically encoded indicators. Proc Natl Acad Sci U S A 2009; 106: 15651–15656. doi:10.1073/pnas.0904764106.
169. Fehr M, Lalonde S, Lager I, Wolff MW, Frommer WB. *In vivo* imaging of the dynamics of glucose uptake in the cytosol of COS-7 cells by fluorescent nanosensors. J Biol Chem 2003; 278: 19127–19133. doi:10.1074/jbc.M301333200.
170. Miyawaki A, Llopis J, Heim R, McCaffery JM, Adams JA, Ikura M, Tsien RY. Fluorescent indicators for Ca^{2+} based on green fluorescent proteins and calmodulin. Nature 1997; 388: 882–887.
171. Vinkenborg JL, Nicolson T, Bellomo EA, Koay MS, Rutter GA, Merkx M. Genetically encoded FRET sensors to monitor Zn^{2+} homeostasis in single cells. Nat Methods 2009; 6: 737–740. doi:10.1038/nmeth.1368.
172. Vinkenborg JL, van Duijnhoven SMJ, Merkx M. Reengineering of a fluorescent zinc sensor protein yields the first genetically encoded cadmium probe. Chem Commun 2011; 47: 11879–11881. doi:10.1039/C1CC14944J.
173. Shi H, He X, Wang K, Wu X, Ye X, Guo Q, Tan W, Qing Z, Yang X, Zhou B. Activatable aptamer probe for contrast-enhanced *in vivo* cancer imaging based on cell membrane protein-triggered conformation alternation. Proc Natl Acad Sci U S A 2011; 108: 3900–3905. doi:10.1073/pnas.1016197108.
174. Yeh HY, Yates MV, Mulchandani A, Chen W. Visualizing the dynamics of viral replication in living cells *via* Tat peptide delivery of nuclease-resistant molecular beacons. Proc Natl Acad Sci U S A 2008; 105: 17522–17525. doi:10.1073/pnas.0807066105.
175. Shimizu Y, Temma T, Hara I, Makino A, Yamahara R, Ozeki E, Ono M, Saji H. Micelle-based activatable probe for *in vivo* near-infrared optical imaging of cancer biomolecules. Nanomedicine 2014; 10: 187–195. doi:10.1016/j.nano.2013.06.009.
176. Tansi FL, Rüger R, Rabenhold M, Steiniger F, Fahr A, Kaiser WA, Hilger I. Liposomal encapsulation of a near-infrared fluorophore enhances fluorescence quenching and reliable whole body optical imaging upon activation *in vivo*. Small 2013; 9: 3659–3669. doi:10.1002/smll.201203211.
177. Tsuji M, Ueda S, Hirayama T, Okuda K, Sakaguchi Y, Isono A, Nagasawa H. FRET-based imaging of transbilayer movement of pepducin in living cells by novel intracellular bioreductively activatable fluorescent probes. Org Biomol Chem 2013; 11: 3030–3037. doi:10.1039/c3ob27445d.
178. Alexander VM, Sano K, Yu Z, Nakajima T, Choyke PL, Ptaszek M, Kobayashi H. Galactosyl human serum albumin-NMP1 conjugate: a near infrared (NIR)-activatable fluorescence imaging agent to detect peritoneal ovarian cancer metastases. Bioconjug Chem 2012; 23: 1671–1679. doi:10.1021/bc3002419.
179. Mitra RN, Doshi M, Zhang X, Tyus JC, Bengtsson N, Fletcher S, Page BD, Turkson J, Gesquiere AJ, Gunning PT, Walter GA, Santra S. An activatable multimodal/multifunctional nanoprobe for direct imaging of intracellular drug delivery. Biomaterials 2012; 33: 1500–1508. doi:10.1016/j.biomaterials.2011.10.068.
180. Solomon M, Guo K, Sudlow GP, Berezin MY, Edwards WB, Achilefu S, Akers WJ. Detection of enzyme activity in orthotopic murine breast cancer by fluorescence lifetime imaging using a fluorescence resonance energy transfer-based molecular probe. J Biomed Opt 2011; 16: 066019. doi:10.1117/1.3594153.
181. Berezin MY, Achilefu S. Fluorescence lifetime measurements and biological imaging. Chem Rev 2010; 110: 2641–2684. doi:10.1021/cr900343z.
182. Goergen CJ, Chen HH, Bogdanov A, Sosnovik DE, Kumar AT. *In vivo* fluorescence lifetime detection of an activatable probe in infarcted myocardium. J Biomed Opt 2012; 17: 056001. doi:10.1117/1.JBO.17.5.056001.
183. Wang TD, Friedland S, Sahbaie P, Soetikno R, Hsiung PL, Liu JT, Crawford JM, Contag CH. Functional imaging of colonic mucosa with a fibered confocal microscope for real-time *in vivo* pathology. Clin Gastroenterol Hepatol 2007; 5: 1300–1305. doi:10.1016/j.cgh.2007.07.013.
184. Zysk AM, Nguyen FT, Oldenburg AL, Marks DL, Boppart SA. Optical coherence tomography: A review of clinical development from

bench to bedside. J Biomed Opt 2007; 12: 051403. doi:10.1117/1.2793736.
185. Wallace MB, Kiesslich R. Advances in endoscopic imaging of colorectal neoplasia. Gastroenterology 2010; 138: 2140–2150. doi:10.1053/j.gastro.2009.12.067.
186. van Dam GM, Themelis G, Crane LMA, Harlaar NJ, Pleijhuis RG, Kelder W, Sarantopoulos A, de Jong JS, Arts HJG, van der Zee AGJ, Bart J, Low PS, Ntziachristos V. Intraoperative tumor-specific fluorescence imaging in ovarian cancer by folate receptor-α targeting: first in-human results. Nat Med 2010; 17: 1315–1319.
187. van der Vorst JR, Schaafsma BE, Hutteman M, Verbeek FP, Liefers GJ, Hartgrink HH, Smit VT, Löwik CW, van de Velde CJ, Frangioni JV, Vahrmeijer AL. Near-infrared fluorescence-guided resection of colorectal liver metastases. Cancer 2013; 119: 3411–3418. doi:10.1002/cncr.28203.
188. Sugie T, Sawada T, Tagaya N, Kinoshita T, Yamagami K, Suwa H, Ikeda T, Yoshimura K, Niimi M, Shimizu A, Toi M. Comparison of the indocyanine green fluorescence and blue dye methods in detection of sentinel lymph nodes in early-stage breast cancer. Ann Surg Oncol 2013; 20: 2213–2218. doi:10.1245/s10434-013-2890-0.
189. Troyan SL, Kianzad V, Gibbs-Strauss SL, Gioux S, Matsui A, Oketokoun R, Ngo L, Khamene A, Azar F, Frangioni JV. The FLARE intraoperative near-infrared fluorescence imaging system: a first-in-human clinical trial in breast cancer sentinel lymph node mapping. Ann Surg Oncol 2009; 16: 2943–2952. doi:10.1245/s10434-009-0594-2.
190. Lee BT, Hutteman M, Gioux S, Stockdale A, Lin SJ, Ngo LH, Frangioni JV. The FLARE intraoperative near-infrared fluorescence imaging system: a first-in-human clinical trial in perforator flap breast reconstruction. Plast Reconstr Surg 2010; 126: 1472–1481. doi:10.1097/PRS.0b013e3181f059c7.
191. Mieog JSD, Troyan SL, Hutteman M, Donohoe KJ, Vorst JR, Stockdale A, Liefers GJ, Choi HS, Gibbs-Strauss SL, Putter H, Gioux S, Kuppen PJ, Ashitate Y, Löwik CW, Smit VT, Oketonoun R, Ngo LH, van de Velde CJ, Frangioni JV, Vahrmeijer AL. Toward optimization of imaging system and lymphatic tracer for near-infrared fluorescent sentinel lymph node mapping in breast cancer. Ann Surg Oncol 2011; 18: 2483–2491. doi:10.1245/s10434-011-1566-x.
192. Fujiwara M, Mizukami T, Suzuki A, Fukamizu H. Sentinel lymph node detection in skin cancer patients using real-time fluorescence navigation with indocyanine green: preliminary experience. J Plast Reconstr Aesthet Surg 2009; 62: e373–e378. doi:10.1016/j.bjps.2007.12.074.
193. van der Vorst JR, Schaafsma BE, Verbeek FPR, Swijnenburg RJ, Hutteman M, Liefers GJ, van de Velde CJ, Frangioni JV, Vahrmeijer AL. Dose optimization for near-infrared fluorescence sentinel lymph node mapping in patients with melanoma. Br J Dermatol 2013; 168: 93–98. doi:10.1111/bjd.12059.
194. Crane LMA, Themelis G, Arts HJG, Buddingh KT, Brouwers AH, Ntziachristos V, van Dam GM, van der Zee AG. Intraoperative near-infrared fluorescence imaging for sentinel lymph node detection in vulvar cancer: first clinical results. Gynecol Oncol 2011; 120: 291–295. doi:10.1016/j.ygyno.2010.10.009.
195. Hutteman M, van der Vorst JR, Gaarenstroom KN, Peters AAW, Mieog JSD, Schaafsma BE, Löwik CW, Frangioni JV, van de Velde CJ, Vahrmeijer AL. Optimization of near-infrared fluorescent sentinel lymph node mapping for vulvar cancer. Am J Obstet Gynecol 2012; 206: 89.e1–5. doi:10.1016/j.ajog.2011.07.039.
196. Crane LM, Themelis G, Pleijhuis RG, Harlaar NJ, Sarantopoulos A, Arts HJ, van der Zee AG, Ntziachristos V, van Dam GM. Intraoperative multispectral fluorescence imaging for the detection of the sentinel lymph node in cervical cancer: a novel concept. Mol Imaging Biol 2011; 13: 1043–1049. doi:10.1007/s11307-010-0425-7.
197. van der Vorst JR, Hutteman M, Gaarenstroom KN, Peters AAW, Mieog JSD, Schaafsma BE, Kuppen PJ, Frangioni JV, van de Velde CJ, Vahrmeijer AL. Optimization of near-infrared fluorescent sentinel lymph node mapping in cervical cancer patients. Int J Gynecol Cancer 2011; 21: 1472–1478. doi:10.1097/IGC.0b013e31822b451d.
198. Vahrmeijer AL, Hutteman M, van der Vorst JR, van de Velde CJH, Frangioni JV. Image-guided cancer surgery using near-infrared fluorescence. Nat Rev Clin Oncol 2013; 10: 507–518. doi:10.1038/nrclinonc.2013.123.
199. Razansky D, Vinegoni C, Ntziachristos V. Multispectral photoacoustic imaging of fluorochromes in small animals. Opt Lett 2007; 32: 2891–2893. doi:10.1364/OL.32.002891.
200. Yao J, Wang LV. Breakthrough in photonics 2013: Photoacoustic tomography in biomedicine. IEEE Photonics J 2014; 6. doi:10.1109/JPHOT.2014.2310197.
201. Razansky D, Harlaar NJ, Hillebrands JK, Taruttis A, Herzog E, Zeebregts CJ, van Dam GM, Ntziachristos V. Multispectral optoacoustic tomography of matrix metalloproteinase activity in vulnerable human carotid plaques. Mol Imaging Biol 2012; 14: 277–285. doi:10.1007/s11307-011-0502-6.
202. Levi J, Kothapalli SR, Ma TJ, Hartman K, Khuri-Yakub BT, Gambhir SS. Design, synthesis, and imaging of an activatable photoacoustic probe. J Am Chem Soc 2010; 132: 11264–11269. doi:10.1021/ja104000a.
203. Levi J, Kothapalli SR, Bohndiek S, Yoon JK, Dragulescu-Andrasi A, Nielsen C, Tisma A, Bodapati S, Gowrishankar G, Yan X, Chan C, Starcevic D, Gambhir SS. Molecular photoacoustic imaging of follicular thyroid carcinoma. Clin Cancer Res 2013; 19: 1494–1502. doi:10.1158/1078-0432.CCR-12-3061.
204. Yang K, Zhu L, Nie L, Sun X, Cheng L, Wu C, Niu G, Chen X, Liu Z. Visualization of protease activity *in vivo* using an activatable photo-acoustic imaging probe based on CuS nanoparticles. Theranostics 2014; 4: 134–141. doi:10.7150/thno.7217.
205. Morgounova E, Shao Q, Hackel BJ, Thomas DD, Ashkenazi S. Photoacoustic lifetime contrast between methylen blue monomers and self-quenched dimers as a model for dual-labeled activatable probes. J Biomed Opt 2013; 18: 056004-1–056004-8.
206. Ashkenazi S. Photoacoustic lifetime imaging of dissolved oxygen using methylene blue. J Biomed Opt 2010; 15: 040501. doi:10.1117/1.3465548.
207. Shao Q, Morgounova E, Jiang C, Choi J, Bischof J, Ashkenazi S. *In vivo* photoacoustic lifetime imaging of tumor hypoxia in small animals. J Biomed Opt 2013; 18: 076019. doi:10.1117/1.JBO.18.7.076019.
208. Strijkers GJ, Nicolay K. Relaxivity of nanoparticles for magnetic resonance imaging. Handbook of Nanophysics: Nanomedicine and Nanorobotics, vol 7, CRC Press: London, 2010.
209. Caravan P, Ellison JJ, McMurry TJ, Lauffer RB. Gadolinium(III) chelates as MRI contrast agents: Structure, dynamics, and applications. Chem Rev 1999; 99: 2293–2352. doi:10.1021/cr980440x.
210. Tu C, Osborne EA, Louie AY. Activatable T_1 and T_2 magnetic resonance imaging contrast agents. Ann Biomed Eng 2011; 39: 1335–1348. doi:10.1007/s10439-011-0270-0.
211. Bonnet CS, Toth E. Smart MR imaging agents relevant to potential neurologic applications. Am J Neuroradiol 2010; 31: 401–409. doi:10.3174/ajnr.A1753.
212. Hingorani DV, Bernstein AS, Pagel MD. A review of responsive MRI contrast agents: 2005–2014. Contrast Media Mol Imaging 2014; online; doi: 10.1102/cmmi.1629
213. Moats RA, Fraser SE, Meade TJ. A "smart" magnetic resonance imaging agent that reports on specific enzymatic activity. Angew Chem Int Ed Engl 1997; 36: 726–728. doi:10.1002/anie.199707261.
214. Urbanczyk-Pearson LM, Femia FJ, Smith J, Parigi G, Duimstra JA, Eckermann AL, Luchinat C, Meade TJ. Mechanistic investigation of β-galactosidase-activated MR contrast agents. Inorg Chem 2008; 47: 56–68. doi:10.1021/ic700888w.
215. Li W, Fraser SE, Meade TJ. A calcium-sensitive magnetic resonance imaging contrast agent. J Am Chem Soc 1999; 121: 1413–1414. doi:10.1021/ja983702l.
216. Hanaoka K, Kikuchi K, Urano Y, Narazaki M, Yokawa T, Sakamoto S, Yamaguchi K, Nagano T. Design and synthesis of a novel magnetic resonance imaging contrast agent for selective sensing of zinc ion. Chem Biol 2002; 9: 1027–1032. doi:10.1016/S1074-5521(02)00216-8.
217. Aime S, Barge A, Botta M, Howard JAK, Kataky R, Lowe MP, Moloney JM, Parker D, de Sousa AS. Dependence of the relaxivity and luminescence of gadolinium and europium amino-acid complexes on hydrogencarbonate and pH. Chem Commun 1999; 11: 1047–1048. doi:10.1039/A902238D.
218. Aime S, Crich SG, Botta M, Giovenzana G, Palmisano G, Sisti M. A macromolecular Gd(III) complex as pH-responsive relaxometric probe for MRI applications. Chem Commun 1999; 16: 1577–1578. doi:10.1039/A900499H.
219. Zhang S, Wu K, Sherry AD. A novel pH-sensitive MRI contrast agent. Angew Chem Int Ed Engl 1999; 38: 3192–3194. doi:10.1002/(SICI)1521-3773(19991102)38:21<3192:AID-ANIE3192>3.0.CO;2-#.
220. Tu C, Louie AY. Photochromically-controlled, reversibly-activated MRI and optical contrast agent. Chem Commun 2007; 13: 1331–1333.

221. Lee T, Zhang X, Dhar S, Faas H, Lippard SJ, Jasanoff A. *In vivo* imaging with a cell-permeable porphyrin-based MRI contrast agent. Chem Biol 2010; 17: 665–673. doi:10.1016/j.chembiol.2010.05.009.
222. Lee YL, Kang HC, Hu J, Nichols JW, Jeon YS, Bae YH. pH-sensitive polymeric micelle-based pH probe for detection and imaging acidic biological environments. Biomacromolecules; 13: 2945–2951; doi: 10.1021/bm300985r
223. Løkling K, Skurtveit R, Bjørnerud A, Fossheim SL. Novel pH-sensitive paramagnetic liposomes with improved MR properties. Magn Reson Med 2004; 51: 688–696. doi:10.1002/mrm.20009.
224. Torres E, Mainini F, Napolitano R, Fedeli F, Cavalli R, Aime S, Terreno E. Improved paramagnetic liposomes for MRI visualization of pH triggered release. J Control Release 2011; 154: 196–202. doi:10.1016/j.conrel.2011.05.017.
225. Santra S, Javita SD, Kaittanis C, Normand G, Grimm J, Perez JM. Gadolinium-encapsulating iron oxide nanoprobe as activatable NMR/MRI contrast agent. ACS Nano 2012; 6: 7281–7294. doi:10.1021/nn302393e.
226. Langereis S, de Lussanet QG, van Genderen MHP, Backes WH, Meijer EW. Multivalent contrast agents based on gadolinium-diethylenetriaminepentaacetic acid-terminated poly(propylene imine) dendrimers for magnetic resonance imaging. Macromolecules 2004; 37: 3084–3091. doi:10.1021/ma035983+.
227. Nivorozhkin AL, Kolodziej AF, Caravan P, Greenfield MT, Lauffer RB, McMurry TJ. Enzyme-activated Gd^{3+} magnetic resonance imaging contrast agents with a prominent receptor-induced magnetization enhancement. Angew Chem Int Ed Engl 2001; 40: 2903–2906. doi:10.1002/1521-3773(20010803)40:15<2903:AID-ANIE2903>3.0.CO;2-N.
228. Hanaoka K, Kikuchi K, Terai T, Komatsu T, Nagano T. A Gd^{3+}-based magnetic resonance imaging contrast agent sensitive to β-galactosidase activity utilizing a receptor-induced magnetization enhancement (RIME) phenomenon. Chemistry 2008; 14: 987–995. doi:10.1002/chem.200700785.
229. Anelli PL, Bertini I, Fragai M, Lattuada L, Luchinat C, Parigi G. Sulfonamide-functionalized gadolinium-DTPA complexes as possible contrast agents for MRI: A relaxometric investigation. Eur J Inorg Chem 2000; 4: 625–630. doi:10.1002/(SICI)1099-0682(200004)2000:4<625:AID-EJIC625>3.0.CO;2–2.
230. Chang YT, Cheng CM, Su YZ, Lee WT, Hsu JS, Liu GC, Cheng TL, Wang YM. Synthesis and characterization of a new bioactivated paramagnetic gadolinium(III) complex [Gd(DOTA-FPG)(H_2O)] for tracing gene expression. Bioconjug Chem 2007; 18: 1716–1727. doi:10.1021/bc070019s.
231. Esqueda AC, López JA, Andreu-de-Riquer G, Alvarado-Monzón JC, Ratnakar J, Lubag AJM, Sherry AD, De León-Rodrigruez LM. A new gadolinium-based MRI zinc sensor. J Am Chem Soc 2009; 131: 11387–11391. doi:10.1021/ja901875v.
232. Querol M, Chen JW, Weissleder R, Bogdanov A Jr. DTPA-bisamide-based MR sensor agents for peroxidase imaging. Org Lett 2005; 7: 1719–1722. doi:10.1021/ol050208v.
233. Nahrendorf M, Sosnovik D, Chen JW, Panizzi P, Figueiredo JL, Aikawa E, Libby P, Swirski FK, Weissleder R. Activatable magnetic resonance imaging agent reports myeloperoxidase activity in healing infarcts and detects the anti-inflammatory effects of atorvastatin on ischemia-reperfusion injury non-invasively. Circulation 2008; 117: 1153–1160. doi:10.1161/CIRCULATIONAHA.107.756510.
234. Bogdanov A Jr, Matuszewski L, Bremer C, Petrovsky A, Weissleder R. Oligomerization of paramagnetic substrates result in signal amplification and can be used for MR imaging of molecular targets. Mol Imaging 2002; 1: 16–23.
235. Querol M, Chen JW, Bogdanov A Jr. A paramagnetic contrast agent with myeloperoxidase-sensing properties. Org Biomol Chem 2006; 4: 1887–1895. doi:10.1039/B601540A.
236. Rodriguez E, Nilges M, Weissleder R, Chen JW. Activatable magnetic resonance imaging agents for myeloperoxidase sensing: Mechanism of activation, stability, and toxicity. J Am Chem Soc 2010; 132: 168–177. doi:10.1021/ja905274f.
237. Thorek DLJ, Chen AK, Czupryna J, Tsourkas A. Superparamagnetic iron oxide nanoparticle probes for molecular imaging. An Biomed Eng 2006; 34: 23–38. doi:10.1007/s10439-005-9002-7.
238. Perez JM, Simeone FJ, Tsourkas A, Josephson L, Weissleder R. Peroxidase substrate nanosensors for MR imaging. Nano Lett 2004; 4: 119–122. doi:10.1021/nl034983k.
239. Harris TJ, von Maltzahn G, Derus A, Ruoslahti E, Bhatia SN. Proteolytic actuation of nanoparticle self-assembly. Angew Chem Int Ed Eng 2006; 45: 3161–3165. doi:10.1002/anie.200600259.
240. von Maltzahn G, Harris TJ, Park JH, Min DH, Schmidt AJ, Sailor MJ, Bhatia SN. Nanoparticle self-assembly gated by logical proteolytic triggers. J Am Chem Soc 2007; 129: 6064–6065. doi:10.1021/ja070461l.
241. Schellenberger E, Rudloff F, Warmuth C, Taupitz M, Hamm B, Schnorr J. Protease-specific nanosensors for magnetic resonance imaging. Bioconjug Chem 2008; 19: 2440–2445. doi:10.1021/bc800330k.
242. Atanasijevic T, Shusteff M, Fam P, Jasanoff A. Calcium-sensitive MRI contrast agents based on superparamagnetic iron oxide nanoparticles and calmodulin. Proc Natl Acad Sci U S A 2006; 103: 14707–14712. doi:10.1073/pnas.0606749103.
243. Perez JM, Josephson L, O'Loughlin T, Högemann D, Weissleder R. Magnetic relaxation switches capable of sensing molecular interactions. Nat Biotechnol 2002; 20: 816–820. doi:10.1038/nbt720.
244. Zhao M, Josephson L, Tang Y, Weissleder R. Magnetic sensors for protease assays. Angew Chem Int Ed Engl 2003; 42: 1375–1378. doi:10.1002/anie.200390352.
245. Perez JM, O'Loughin T, Simeone FJ, Weissleder R, Josephson L. DNA-based magnetic nanoparticle assembly acts as a magnetic relaxation nanoswitch allowing screening of DNA-cleaving agents. J Am Chem Soc 2002; 124: 2856–2857. doi:10.1021/ja017773n.
246. Granot D, Shapiro EM. Release activation of iron oxide nanoparticles: (REACTION) A novel environmentally sensitive MRI paradigm. Magn Reson Med 2011; 65: 1253–1259.
247. Viswanathan S, Kovacs Z, Green KN, Ratnakar J, Sherry AD. Alternatives to gadolinium-based metal chelates for magnetic resonance imaging. Chem Rev 2010; 110: 2960–3018. doi:10.1021/cr900284a.
248. Yoo B, Sheth VR, Howison CM, Douglas MJK, Pineda CT, Maine EA, Baker AF, Pagel MD. Detection of *in vivo* enzyme activity with CatalyCEST MRI. Magn Res Med 2014; 71: 1221–1230. doi:10.1002/mrm.24763.
249. Tsitovich PB, Spernyak JA, Morrow JR. A redox-activated MRI contrast agent that switches between paramagnetic and diamagnetic states. Angew Chem Int Ed 2013; 52: 13997–14000. doi:10.1002/anie.201306394.
250. Aime S, Barge A, Castelli DD, Fedeli F, Mortillaro A, Nielsen FU, Terreno E. Paramagnetic lanthanide(III) complexes as pH-sensitive chemical exchange saturation transfer (CEST) contrast agents for MRI applications. Magn Reson Med 2002; 47: 639–648. doi:10.1002/mrm.10106.
251. Mikawa M, Miwa N, Bräutigan M, Akaike T, Maruyama A. A pH-sensitive contrast agent for functional magnetic resonance imaging (MRI). Chem Lett 1998; 27: 693–694. doi:10.1246/cl.1998.693.
252. Hovland R, Gløgård C, Aasen AJ, Klaveness J. Preparation and *in vitro* evaluation of a novel amphiphilic GdPCTA-[12] derivative; a micellar MRI contrast agent. Org Biomol Chem 2003; 1: 644–647. doi:10.1039/B211039C.
253. Aime S, Castelli DD, Terreno E. Novel pH-reporter MRI contrast agents. Angew Chem Int Ed Engl 2002; 41: 4334–4336. doi:10.1002/1521-3773(20021115)41:22<4334:AID-ANIE4334>3.0.CO;2–1.
254. Pikkemaat JA, Wegh RT, Lamerichs R, van de Molengraaf RA, Langereis S, Burdinski D, Raymond AY, Janssen HM, de Waal BF, Willard NP, Meijer EW, Grüll H. Dendritic PARACEST contrast agents for magnetic resonance imaging. Contrast Media Mol Imaging 2007; 2: 229–239. doi:10.1002/cmmi.149.
255. Yoo B, Pagel MD. A PARACEST MRI contrast agent to detect enzyme activity. J Am Chem Soc 2006; 128: 14032–14033. doi:10.1021/ja063874f.
256. Li Y, Sheth VR, Liu G, Pagel MD. A self-calibrating PARACEST MRI contrast agent that detects esterase enzyme activity. Contrast Media Mol Imaging 2011; 6: 219–228. doi:10.1002/cmmi.421.
257. Aime S, Castelli DD, Fedeli F, Terreno E. A Paramagnetic MRI-CEST agent responsive to lactate concentration. J Am Chem Soc 2002; 124: 9364–9365.
258. Angelovski G, Chauvin T, Pohmann R, Logothetis NK, Toth E. Calcium-responsive paramagnetic CEST agents. Bioorg Med Chem 2011; 19: 1097–1105. doi:10.1016/j.bmc.2010.07.023.
259. Ratnakar SJ, Viswanathan S, Kovacs Z, Jindal AK, Green KN, Sherry AD. Europium(III) DOTA-tetraamide complexes as redox-active MRI

sensors. J Am Chem Soc 2012; 134: 5798–5800. doi:10.1021/ja211601k.
260. Liu G, Li Y, Pagel MD. Design and characterization of a new irreversible responsive PARACEST MRI contrast agent that detects nitric oxide. Magn Res Med 2007; 58: 1249–1256.
261. Zhang S, Trokowski R, Sherry AD. A paramagnetic CEST agent for imaging glucose by MRI. J Am Chem Soc 2003; 125: 15288–15289.
262. Chauvin T, Durand P, Bernier M, Meudal H, Doan BT, Noury F, Badet B, Beloeil JC, Tóth E. Detection of enzymatic activity by PARACEST MRI: A general approach to target a large variety of enzymes. Angew Chem Int Ed Engl 2008; 47: 4370–4372. doi:10.1002/anie.200800809.
263. Ratnakar SJ, Soesbe TC, Lumata LL, Do QN, Viswanathan S, Lin CY, Sherry AD, Kovacs Z. Modulation of CEST images *in vivo* by T1 relaxation: A new approach in the design of responsive PARACEST agents. J Am Chem Soc 2013; 135: 14904–14907.
264. Kurhanewicz J, Vigneron DB, Brindle K, Chekmenev EY, Comment A, Cunningham CH, DeBerardinis RJ, Green GG, Leach MO, Rajan SS, Rizi RR, Ross BD, Warren WS, Malloy CR. Analysis of cancer metabolism by imaging hyperpolarized nuclei: Prospects for translation to clinical research. Neoplasia 2011; 13: 81–97.
265. Cabella C, Karlsson M, Canape C, Catanzaro G, Colombo Serra S, Miragoli L, Poggi L, Uggeri F, Venturi L, Jensen PR, Lerche MH, Tedoldi F. *In vivo* and *in vitro* liver cancer metabolism observed with hyperpolarized [5–13C]glutamine. J Magn Res 2013; 232: 45–52.
266. Nelson SJ, Kurhanewicz J, Vigneron DB, Larson PEZ, Harzstark AL, Ferrone M, van Criekinge M, Chang JW, Bok R, Park I, Reed G, Carvajal L, Small EJ, Munster P, Weinberg VK, Ardenkjaer-Larsen JH, Chen AP, Hurd RE, Odegardstuen L, Robb FJ, Tropp J, Murray JA. Metabolic imaging of patients with prostate cancer using hyperpolarized [1-^{13}C]pyruvate. Sci Trans Med 2013; 5: 198ra108
267. Lee S, Park K, Kim K, Choi K, Kwon IC. Activatable imaging probes with amplified fluorescent signals. Chem Commun 2008: 4250–4260. doi:10.1039/B806854M.
268. Teesalu T, Sugahara KN, Kotamraju VR, Ruoslahti E. C-end rule peptides mediate neuropilin-1-dependent cell, vascular, and tissue penetration. Proc Natl Acad Sci U S A 2009; 106: 16157–16162. doi:10.1073/pnas.0908201106.
269. Sugahara KN, Teesalu T, Karmali PP, Kotamraju VR, Agemy L, Girard OM, Hanahan D, Mattrey RF, Ruoslahti E. Tissue-penetrating delivery of compounds and nanoparticles into tumors. Cancer Cell 2009; 16: 510–520. doi:10.1016/j.ccr.2009.10.013.
270. Jaffer FA, Tung CH, Wykrzykowska JJ, Ho NH, Houng AK, Reed GL, Weissleder R. Molecular imaging of factor XIIIa activity in thrombosis using a novel, near-infrared fluorescent contrast agent that covalently links to thrombi. Circulation 2004; 110: 170–176. doi:10.1161/01.CIR.0000134484.11052.44.
271. Kim DE, Schellingerhout D, Jaffer FA, Weissleder R, Tung CH. Near-infrared fluorescent imaging of cerebral thrombi and blood–brain barrier disruption in a mouse model of cerebral venous sinus thrombosis. J Cereb Blood Flow Metab 2005; 25: 226–233. doi:10.1038/sj.jcbfm.9600023.
272. Miserus RJHM, Herías V, Prinzen L, Lobbes MB, Van Suylen RJ, Dirksen A, Hackeng TM, Heemskerk JW, van Engelshoven JM, Daemen MJ, van Zandvoort MA, Heeneman S, Kooi ME. Molecular MRI of early thrombus formation using a bimodal alpha2-antiplasmin-based contrast agent. JACC Cardiovasc Imaging 2009; 2: 987–996. doi:10.1016/j.jcmg.2009.03.015.
273. Nahrendorf M, Hu K, Frantz S, Jaffer FA, Tung CH, Killer KH, Voll S, Nordbeck P, Sosnovik D, Gattenlöhner S, Novikov M, Dickneite G, Reed GL, Jakob P, Rosenzweig A, Bauer WR, Weissleder R, Ertl G. Factor XIII deficiency causes cardiac rupture, impairs wound healing, and aggravates cardiac remodeling in mice with myocardial infarction. Circulation 2006; 113: 1196–1202. doi:10.1161/CIRCULATIONAHA.105.602094.
274. Nahrendorf M, Aikawa E, Figueiredo JL, Stangenberg L, van den Borne SW, Blankesteijn WM, Sosnovik DE, Jaffer FA, Tung CH, Weissleder R. Transglutaminase activity in acute infarcts predicts healing outcome and left ventricular remodelling: Implications for FXIII therapy and antithrombin use in myocardial infarction. Eur Heart J 2008; 29: 445–454. doi:10.1093/eurheartj/ehm558.
275. Loving GS, Caravan P. Activation and retention: a magnetic resonance probe for detection of acute thrombosis. Angew Chem Int Ed Engl 2014; 53: 1140–1143. doi:10.1002/anie.201308607.
276. Westmeyer GG, Emer Y, Lintelmann J, Jasanoff A. MRI-based detection of alkanine phosphatase gene reporter activity using a porphyrin solubility switch. Chem Biol 2014; 21: 422–429. doi:10.1016/j.chembiol.2014.01.012.
277. Pauwels EKJ, Ribeiro MJ, Stoot JH, McCready VR, Bourguignon M, Mazière B. FDG accumulation and tumor biology. Nucl Med Biol 1998; 25: 317–322.
278. Been LB, Suurmeijer AJH, Cobben DCP, Jager PL, Hoekstra HJ, Elsinga PH. [^{18}F]-FLT-PET in oncology: current status and opportunities. Eur J Nucl Med Mol Imaging 2004; 31: 1659–1672. doi:10.1007/s00259-004-1687-6.
279. DeGrado TR, Baldwin SW, Wang S, Orr MD, Liao RP, Friedman HS, Reiman R, Price DT, Coleman RE. Synthesis and evaluation of 18F-labeled choline analogs as oncologic PET tracers. J Nucl Med 2001; 42: 1805–1814.
280. Brogsitter C, Zöphel K, Kotzerke J. 18F-choline, 11C-choline and 11C-acetate PET/CT: comparative analysis for imaging prostate cancer patients. Eur J Nucl Med Mol Imaging 2013; 40: S18–S27. doi:10.1007/s00259-013-2358-2.
281. Sanghera B, Wong WL, Sonoda LI, Beynon G, Makris A, Woolf D, Ardeshna K. FLT PET-CT in evaluation of treatment response. Indian J Nucl Med 2014; 29: 65–73. doi:10.4103/0972-3919.130274.
282. Carroll V, Michel BW, Blecha J, VanBrocklin H, Keshari K, Wilson D, Chang CJ. A boronate-caged [18F]FLT probe for hydrogen peroxide detection using positron emission tomography. J Am Chem Soc 2014; 136: 14742–14745. doi:10.1021/ja509198w.
283. Thorek DL, Ogirala A, Beattie BJ, Grimm J. Quantitative imaging of disease signatures through radioactive decay signal conversion. Nat Med 2013; 13: 1345–1350. doi:10.1038/nm.3323.
284. Tjuvajev JG, Doubrovin M, Akhurst T, Cai S, Balatoni J, Alauddin MM, Finn R, Bornmann W, Thaler H, Conti PS, Blasberg RG. Comparison of radiolabeled nucleoside probes (FIAU, FHBG, and FHPG) for PET imaging of HSV1-tk gene expression. J Nucl Med 2002; 43: 1072–1083.
285. Choi SR, Zhuang ZP, Chacko AM, Acton PD, Tjuvajev-Gelovnani J, Chu DC, Kung HF. SPECT imaging of herpes simplex virus type1 thymidine kinase gene expression by [(123}I]FIAU(1). Acad Radiol 2005; 12: 798–805. doi:10.1016/j.acra.2005.04.010.
286. Jacobs A, Voges J, Reszka R, Lercher M, Gossmann A, Kracht L, Kaestle C, Wagner R, Wienhard K, Heiss WD. Positron-emission tomography of vector-mediated gene expression in gene therapy for gliomas. Lancet 2001; 358: 727–729.
287. Wilson TA, Karajannis MA, Harter DH. Glioblastoma multiforme: State of the art and future therapeutics. Surg Neurol Int 2014; 5: 64. doi:10.4103/2152-7806.132138.
288. Zhang Q, Liu H, Pan Z. A general approach for the development of fluorogenic probes suitable for no-wash imaging of kinases in live cells. Chem Commun 2014; 50: 15319–15322. doi:10.1039/c4cc07429g.
289. Bauer C, Bauder-Wuest U, Mier W, Haberkorn U, Eisenhut M. 131I-labeled peptides as caspase substrates for apoptosis imaging. J Nucl Med 2005; 46: 1066–1074.
290. Bohn P, Mouchard F, Rouvet J, de Boisgrollier A, Vera P. 99mTc-(Me)FGCDEVD, a potential tracer for apoptosis detection. Bioorg Med Chem Lett 2013; 23: 1375–1378. doi:10.1016/j.bmcl.2012.12.088.
291. Xie R, Dong L, Huang R, Hong S, Lei R, Chen X. Targeted imaging and proteomic analysis of tumor-associated glycans in living animals. Angew Chem Int Ed 2014; 53: 14082–14086. doi:10.1002/anie.201408442.
292. Chang PV, Prescher JA, Hangauer MJ, Bertozzi CR. Imaging cell surface glycans with bioorthogonal chemical reporters. J Am Chem Soc 2007; 129: 8400–8401. doi:10.1021/ja070238o.
293. Neves AA, Stöckmann H, Wainman YA, Kuo JCH, Fawcett S, Leeper FJ, Brindle KM. Imaging cell surface glycosylation *in vivo* using "double click" chemistry. Bioconjug Chem 2013; 24: 934–941. doi:10.1021/bc300621n.
294. Laughlin ST, Baskin JM, Amacher SL, Bertozzi CR. *In vivo* imaging of membrane-associated glycans in developing zebrafish. Science 2008; 320: 664–667. doi:10.1126/science.1155106.
295. Ouahab A, Cheraga N, Onoja V, Shen Y, Tu J. Novel pH-sensitive charge-reversal cell penetrating peptide conjugated PEG-PLA micelles for docetaxel delivery: *in vitro* study. Int J Pharm 2014; 466: 233–245. doi:10.1016/j.ijpharm.2014.03.009.
296. Gao GH, Lee JW, Nguyen MK, Im GH, Yang J, Heo H, Jeon P, Park TG, Lee JH, Lee DS. pH-responsive polymeric micelle based on

PEG-poly(β-aminoester)/(amido amine) as intelligent vehicle for magnetic resonance imaging in detection of cerebral ischemic area. J Control Release 2011; 155: 11–17. doi:10.1016/j.conrel.2010.09.012.
297. Andreev OA, Dupuy AD, Segala M, Sandugu S, Serra DA, Chichester CO, Engelman DM, Reshetnyak YK. Mechanism and uses of a membrane peptide that targets tumors and other acidic tissues *in vivo* . Proc Natl Acad Sci U S A 2007; 104: 7893–7898; doi: 10.1073/pnas.0702439104
298. Vävere AL, Biddlecombe GB, Spees WM, Garbow JR, Wijesinghe D, Andreev OA, Engelman DM, Reshetnyak YK, Lewis JS. A novel technology for the imaging of acidic prostate tumors by positron emission tomography. Cancer Res 2009; 69: 4510–4516. doi:10.1158/0008-5472.CAN-08-3781.
299. Lopci E, Grassi I, Chiti A, Nanni C, Cicoria G, Toschi L, Fonti C, Lodi F, Mattioli S, Fanti S. PET radiopharmaceuticals for imaging of hypoxia: a review of the evidence. Am J Nucl Med Mol Imaging 2014; 4: 365–384.
300. Hsia C, Huang F, Hung G, Shen L, Chen C, Wang H. The biological characterization of 99mTc-BnAO-NI as a SPECT probe for imaging hypoxia in a sarcoma-bearing mouse model. Appl Rad Isot 2011; 69: 649–655.
301. Takasawa M, Moustafa RR, Baron JC. Applications of nitroimidazole *in vivo* hypoxia imaging in ischemic stroke. Stroke 2008; 39: 1629–1637. doi:10.1161/STROKEAHA.107.485938.
302. Rischin D, Hicks RJ, Fisher R, Binns D, Corry J. Porceddu S, Peter LJ, Trans-Tasman-Radiation Oncology Group Study 98.02. Prognostic significance of [18F]-misonidazole positron emission tomography-detected tumor hypoxia in patients with advanced head and neck cancer randomly assigned to chemoradiation with or without tirapazamine: a substudy of Trans–Tasman Radiation Oncology Group Study 98.02. J Clin Oncol 2006; 24: 2098–2104.
303. Peeters SG, Zeger CM, Lieuwes NG, van Elmpt W, Eriksson J, van Dongen GAMS, Dubois L, Lambin P. A comparative study of the hypoxia PET tracers [^{18}F]HX4, [^{18}F]FAZA, and [^{18}F]FMISO in a preclinical tumor model. Int J Radiation Oncol Biol Phys 2014; S0360-3016(14): 04198–4. doi:10.1016/j.ijrobp.2014.09.045.
304. Mortensen LS, Johansen J, Kallehauge J, Primdahl H, Busk M, Lassen P, Alsner J, Sorensen BS, Toustrup K, Jakobsen S, Petersen J, Petersen H, Theil J, Nordsmark M, Overgaard J. FAZA PET/CT hypoxia imaging in patients with squamous cell carcinoma of the head and neck treated with radiotherapy: results from the DAHANCA 24 trial. Radiother Oncol 2012; 105: 14–20. doi:10.1016/j.radonc.2012.09.015.
305. Chen L, Zhang Z, Kolb HC, Walsh JC, Zhang J, Guan Y. ^{18}F-HX4 hypoxia imaging with PET/CT in head and neck cancer: a comparison with ^{18}F-FMISO. Nucl Med Commun 2012; 33: 1096–1102. doi:10.1097/MNM.0b013e3283571016.
306. Hueting R, Kersemans V, Cornelissen B, Tredwell M, Hussien K, Christlieb M, Gee AD, Passier J, Smart SC, Dilworth JR, Gouverneur V, Muschel RJ. A comparison of the behaviour of ^{64}Cu-actetate and ^{64}Cu-ATSM *in vitro* and *in vivo*. J Nucl Med 2014; 55: 128–134. doi:10.2967/jnumed.113.119917.
307. Ikawa M, Okazawa H, Kudo T, Kuriyama M, Fujibayashi Y, Yoneda M. Evaluation of striatal oxidative stress in patients with Parkinson's disease using [62Cu]ATSM PET. Nucl Med Biol 2011; 38: 945–951. doi:10.1016/j.nucmedbio.2011.02.016.
308. Kimura S, Umeda IO, Moriyama N, Fujii H. Syntesis and evaluation of a novel 99mTc-labeled bioreductive probe for tumor hypoxia imaging. Bioorg Med Chem Lett 2011; 21: 7359–7362.
309. Ueda M, Ogawa K, Miyano A, Ono M, Kizaka-Kondoh S, Saji H. Development of an oxygen-sensitive degradable peptide probe for the imaging of hypoxia-inducible factor-1-active regions in tumors. Mol Imaging Biol 2013; 15: 713–721. doi:10.1007/s11307-013-0647-6.
310. Lepage M, Dow WC, Melchior M, You Y, Fingleton B, Quarles CC, Pépin C, Gore JC, Matrisian LM, McIntyre JO. Noninvasive detection of matrix metalloproteinase activity *in vivo* using a novel MRI contrast agent with a solubility switch. Mol Imaging 2007; 6: 393–403.
311. Lebel R, Jastrzebska B, Therriault H, Cournoyer MM, McIntyre JO, Escher E, Neugebauer W, Paguette B, Lepage M. Novel solubility-switchable MRI agent allows the noninvasive detection of matrix metalloproteinase-2 activity *in vivo* in a mouse model. Mag Res Med 2008; 60: 1056–1065. doi:10.1002/mrm.21741.
312. Jastrzebska B, Lebel R, Therriault H, McIntyre JO, Escher E, Guérin B, Paguette B, Neugebauer WA, Lepage M. New enzyme-activated solubility-switchable contrast agent for magnetic resonance imaging: From synthesis to *in vivo* imaging. J Med Chem 2009; 52: 1576–1581. doi:10.1021/jm801411h.
313. Chuang CH, Chuang KH, Wang HE, Roffler SR, Shiea JT, Tzou SC, Cheng TC, Kao CH, Wu SY, Tseng WL, Cheng CM, Hou MF, Wang JM, Cheng TL. *In vivo* positron emission tomography imaging of protease activity by generation of a hydrophobic product from a noninhibitory protease substrate. Clin Cancer Res 2012 ; 18 : 238–247; doi: 10.1158/1078-0432.CCR-11-0608
314. Jiang T, Olson ES, Nguyen QT, Roy M, Jennings PA, Tsien RY. Tumor imaging by means of proteolytic activation of cell-penetrating peptides. Proc Natl Acad Sci U S A 2004; 101: 17867–17872. doi:10.1073/pnas.0408191101.
315. Aguilera TA, Olson ES, Timmers MM, Jiang T, Tsien RY. Systemic *in vivo* distribution of activatable cell penetrating peptides is superior to that of cell penetrating peptides. Integr Biol 2009; 1: 371–381. doi:10.1039/B904878B.
316. Olson ES, Aguilera TA, Jiang T, Ellies LG, Nguyen QT, Wong EH, Gross LA, Tsien RY. *In vivo* characterization of activatable cell penetrating peptides for targeting protease activity in cancer. Integr Biol 2009; 1: 382–393. doi:10.1039/B904890A.
317. Olson ES, Jiang T, Aguilera TA, Nguyen QT, Ellies LG, Scadeng M, Tsien RY. Activatable cell penetrating peptides linked to nanoparticles as dual probes for *in vivo* vluorescence and MR imaging of proteases. Proc Natl Acad Sci U S A 2010; 107: 4311–4316. doi:10.1073/pnas.0910283107.
318. Nguyen QT, Olson ES, Aguilera TA, Jiang T, Scadeng M, Ellies LG, Tsien RY. Surgery with molecular fluorescence imaging using activatable cell-penetrating peptides decreases residual cancer and improves survival. Proc Natl Acad Sci U S A 2010; 107: 4317–4322. doi:10.1073/pnas.0910261107.
319. Savariar EN, Felsen CN, Nashi N, Jiang T, Ellies LG, Steinbach P, Tsien RY, Nguyen QT. Real-time *in vivo* molecular detection of primary tumors and metastasis with ratiometric activatable cell-penetrating peptides. Cancer Res 2013; 73: 855–864. doi:10.1158/0008-5472.CAN-12-2969.
320. van Duijnhoven SMJ, Robillard MS, Nicolay K, Grüll H. Tumor targeting of MMP-2/9 activatable cell-penetrating imaging probes is caused by tumor-independent activation. J Nucl Med 2011; 52: 279–286. doi:10.2967/jnumed.110.082503.
321. van Duijnhoven SMJ, Robillard MS, Nicolay K, Grüll H. *In vivo* biodistribution of radiolabeled MMP-2/9 activatable cell-penetrating peptide probes in tumor-bearing mice. Contrast Media Mol Imaging 2014. Epub ahead of print; doi: 10.1002/cmmi.1605
322. Xia Z, Xing Y, Jeon J, Kim YP, Gall J, Dragulescu-Andrasi A, Gambhir SS, Rao J. Immobilizing reporters for molecular imaging of the extracellular microenvironment in living animals. ACS Chem Biol 2011; 6: 1117–1126. doi:10.1021/cb200135e.
323. van Duijnhoven SMJ, Robillard MS, Hermann S, Kuhlmann MT, Schäfers M, Nicolay K, Grüll H. Imaging of MMP activity in postischemic cardiac remodeling using radiolabeled MMP-2/9 activatable cell-penetrating imaging probes. Mol Pharmaceutics 2014; 11: 1415–1423. doi:10.1021/mp400569k.
324. Felsen CN, Savariar EN, Whitney M, Tsien RY. Detection and monitoring of localized matrix metalloproteinase upregulation in a murine model of asthma. Am J Physiol Lung Cell Mol Physiol 2014; 306: L764–L774. doi:10.1152/ajplung.00371.2013.
325. Goun EA, Shinde R, Dehnert KW, Adams-Bond A, Wender PA, Contag CH, Franc BL. Intracellular cargo delivery by an octaarginine transporter adapted to target prostate cancer cells through cell surface protease activation. Bioconjug Chem 2006; 17: 787–796. doi:10.1021/bc0503216.
326. Yuan X, Lin X, Manorek G, Howell SB. Challenges associated with the targeted delivery of gelonin to claudin expressing cancer cells with the use of activatable cell penetrating peptides to enhance potency. BMC Cancer 2011; 11: 61–70. doi:10.1186/1471-11-61.
327. Watkins GA, Jones EF, Shell MS, VanBrocklin HF, Pan MH, Hanrahan SM, Feng JJ, He J, Sounni NE, Dill KA, Contag CH, Coussens LM, Franc BL. Development of an optimized activatable MMP-14 targeted SPECT imaging probe. Bioorg Med Chem 2009; 17: 653–659. doi:10.1016/j.bmc.2008.11.078.

328. Whitney M, Crisp JL, Olson ES, Aguilera TA, Gross LA, Ellies LG, Tsien RY. Parallel *in vivo* and *in vitro* selection using phage display identifies protease dependent tumor targeting peptides. J Biol Chem 2010; 285: 22532–22541. doi:10.1074/jbc.M110.138297.
329. Chen J, Liu TWB, Lo PC, Wilson BC, Zheng G. Zipper molecular beacons: A generalized strategy to optimize the performance of activatable protease probes. Bioconjug Chem 2009; 20: 1836–1842. doi:10.1021/bc900207k.
330. Olson ES, Whitney MA, Friedman B, Aguilera TA, Crisp JL, Baik FM, Jiang T, Baird SM, Tsimikas S, Tsien RY, Nguyen QT. *In vivo* fluorescence imaging of atherosclerotic plaques with activatable cell-penetrating peptides targeting thrombin activity. Integr Biol 2012; 4: 595–605. doi:10.1039/C2IB00161F.
331. Whitney M, Savariar EN, Friedman B, Levin RA, Crisp JL, Glasgow HL, Lefkowitz R, Adams SR, Steinbach P, Nashi N, Nguyen QT, Tsien RY. Ratiometric activatable cell-penetrating peptides provide rapid *in vivo* readout of thrombin activation. Angew Chem Int Ed Engl 2013; 52: 325–330. doi:10.1002/anie.201205721.
332. Zhang Y, So MK, Rao J. Protease-modulated cellular uptake of quantum dots. Nano Lett 2006; 6: 1988–1992. doi:10.1021/nl0611586.
333. Mok H, Bae KH, Ahn CH, Park TG. PEGylated and MMP-2 specifically dePEGylated quantum dots: Comparative evaluation of cellular uptake. Langmuir 2009; 25: 1645–1650. doi:10.1021/la803542v.
334. Liang G, Ren H, Rao J. A biocompatible condensation reaction for controlled assembly of nanostructures in living cells. Nat Chem 2010; 2: 54–60. doi:10.1038/nchem.480.
335. Dragulescu-Andrasi A, Kothapalli SR, Tikhomirov GA, Rao J, Gambhir SS. Activatable oligomerizable imaging agents for photoacoustic imaging of furin-like activity in living subjects. J Am Chem Soc 2013; 135: 11015–110122. doi:10.1021/ja40100078.
336. Cobos-Correa A, Trojanek JB, Diemer S, Mall MA, Schultz C. Membrane-bound FRET probe visualizes MMP-12 activity in pulmonary inflammation. Nat Chem Biol 2009; 5: 628–630. doi:10.1038/nchembio.196.
337. Zhao T, Harada H, Teramura Y, Tanaka S, Itasaka S, Morinibu A, Shinomiya K, Zhu Y, Hanaoka H, Iwata H, Saji H, Hiraoka M. A novel strategy to tag matrix metalloproteinases-positive cells for *in vivo* imaging of invasive and metastatic activity of tumor cells. J Control Release 2010; 144: 109–114. doi:10.1016/j.conrel.2010.01.023339.
338. Suzuki H, Sato M, Umezawa Y. Accurate targeting of activated macrophages based on synergistic activation of functional molecules uptake by scavenger receptor and matrix metalloproteinase. ACS Chem Biol 2008; 3: 471–479. doi:10.1021/cb800067e.
339. Breurken M, Lempens EHM, Merkx M. Protease-activatable collagen targeting based on protein cyclization. ChemBioChem 2010; 11: 1165–1168. doi:10.1002/cbic.201000223.
340. Breurken M, Lempens EHM, Meijer EW, Merkx M. Semi-synthesis of a protease-activatable collagen targeting probe. Chem Commun 2011; 47: 7998–8000. doi:10.1039/c1cc11964h.